3-22-2012

OFDM-Based Signal Exploitation Using Quadrature Mirror Filter Bank (QMFB) Processing

Felipe E. Garrido

OFDM-BASED SIGNAL EXPLOTATION USING QUADRATURE MIRROR FILTER BANK (QMFB) PROCESSING

THESIS

Felipe E. Garrido, Captain, Chilean Air Force

AFIT/GE/ENG/12-16

DEPARTMENT OF THE AIR FORCE
AIR UNIVERSITY

AIR FORCE INSTITUTE OF TECHNOLOGY

Wright-Patterson Air Force Base, Ohio

AFIT/GE/ENG/12-16

OFDM-BASED SIGNAL EXPLOTATION USING QUADRATURE MIRROR FILTER BANK (QMFB) PROCESSING

THESIS

Presented to the Faculty

Department of Electrical and Computer Engineering

Graduate School of Engineering and Management

Air Force Institute of Technology

Air University

Air Education and Training Command

In Partial Fulfillment of the Requirements for the

Degree of Master of Science

Felipe E. Garrido, E.E.

Captain, Chilean Air Force

March 2012

AFIT/GE/ENG/12-16

OFDM-BASED SIGNAL EXPLOTATION USING QUADRATURE MIRROR FILTER BANK (QMFB) PROCESSING

Felipe E. Garrido, E.E.
Captain, Chilean Air Force

Approved:

Michael A. Temple, Ph.D. (Chairman) — 1 Mar 2012 — Date

Geoffrey A. Akers, Ph.D. (Member) — 29 Feb 2012 — Date

Peter J. Collins, Ph.D. (Member) — 29 FEB 2012 — Date

AFIT/GE/ENG/12-16

Abstract

By performing Quadrature Mirror Filter Bank (QMFB) processing with a given signal it is possible to obtain Frequency-Time (F-T) outputs that represent signal features such as bandwidth (W), center frequency (f_c), signal duration (T_s), modulation type (AM, FM, BPSK, QAM, etc), frequency content and time allocation. Because of its unique structure, two widely used signals based on Orthogonal Frequency Division Multiplexing (OFDM) were chosen as signals of interest for demonstration. The general implementation of the QMFB process is described along with the basic structure of OFDM signals related to the physical layer perspective of 802.11a Wi-Fi and 802.16e WiMAX frame structures are described.

The adopted methodology is aimed at exploiting signal of interest features accounting for the effects of signal resampling and zero-padding. Computed simulation results are obtained after applying the defined methodology to each signal of interest. Initial time domain and frequency domain responses are presented for each input signal along with the initial and computed resampled parameters for each case. Results for selected QMFB outputs are presented using 2D F-T QMFB plots and 1D average frequency and average time plots. These plots enable qualitative visual assessment such as may be used by a human operator. The 1D responses are computed for the input signal and output QMFB responses and compared using overlay plots for single burst and multiple integrated burst inputs. Resultant time (Δt) and frequency (Δf) resolutions were consistent and validate the usefulness of QMFB processing.

To my father's memory:

I cannot think of any need in childhood as strong as the need for a father's protection.

Sigmund Freud

Acknowledgments

First I would like to thank to my advisor Dr. Michael Temple who has supported me during this complete process since the first quarter at AFIT. This thesis would not be possible without his guidance, encouragement and effort.

To my girlfriend and all of my friends in Chile, I want to thank you for always wishing me the best and because the distance has not been a barrier to remain together.

To the Chilean Air Force that trusted in me to accomplish this challenge and especially to the liaison officers who always had a place for me in their office and more importantly in their homes.

To all who are part of IMSO because you have been an essential support during this experience and integration within AFIT.

To all AFIT teachers who, regardless of the language differences, always had time to answer my many questions.

To all of my classmates and especially the guys in RAIL, because you were always available to help me and you all have been a real inspiration to improve my work.

Finally and foremost to my family who, despite the distance, have been my daily support and the main reason I am able to achieve my goals.

Felipe E. Garrido

Table of Contents

Page

List of Figures

List of Tables

List of Acronyms

AGC	Automatic Gain Control
AM	Amplitude Modulation
BPSK	Binary Phase Shift Keying
BS	Base Station
CW	Continuous Wave
DL	Down Link
DMT	Discrete Multi Tone
FDD	Frequency Division Duplexing
FDM	Frequency Division Multiplexing
FFT	Fast Fourier Transform
FM	Frequency Modulation
FMCW	Frequency Modulated Continuous Wave
FSK	Frequency Shift Keying
F-T	Frequency-Time
G-M	Gronholz-Mims
LAN	Local Area Network
LFM	Linear Frequency Modulation
MS	Mobile Subscriber
NoNET	Noise Network
NTR	Noise Technology Radar
OFDM	Orthogonal Frequency Modulation

PLCP	Physical Layer Convergence Procedure
PPDU	PLCP Protocol Data Unit
PSD	Power Spectral Density
PSDU	PLCP Service Data Unit
PSK	Phase Shift Keying
QAM	Quadrature Amplitude Modulation
QMFB	Quadrature Mirror Filter Bank
QPSK	Quadrature Phase Shift Keying
RF	Radio Frequency
RF-DNA	RF-Distinct Native Attribute
RFSICS	RF-Signal Intercept and Collection System
SS	Subscriber Station
TDD	Time Division Multiplexing
UL	Up Link
V&V	Verification and Validation
W	Bandwidth
Wi-Fi	Wireless Fidelity
WiMAX	Worldwide Interoperability for Microwave Access
WLAN	Wide Local Area Network

OFDM-BASED SIGNAL EXPLOTATION USING QUADRATURE MIRROR FILTER BANK (QMFB) PROCESSING

CHAPTER 1.
Introduction

This chapter presents the research motivation, research objectives and research organization. The research motivation is divided in two subsections aimed to provide the operational motivation (Section 1.1.1) and the technical motivation (Section 1.1.2) for the research effort. Research objectives are defined in Section 1.2.3 with a goal of 1) finding empirical results aimed at satisfying the research motivation, and 2) finding a graphical representation that is useful for highlighting discriminating signal features from an operators' perspective. Finally, the research organization is presented in Section 1.2.4.

1.1 Research Motivation

1.1.1 Operational Motivation

Previous related work with Quadrature Mirror Filter Bank (QMFB) processing [1, 3, 4] has demonstrated some practical capability for exploiting a given signal by using resultant frequency-time (F-T) plots to highlight some signal's distinctive characteristics. Other signal exploitation procedures using passive methods are given in [8], which is based on performing wavelet-based radio frequency (RF) fingerprinting, and [0, 11] which is based on performing Gabor-Based RF Distinct Native Attribute (DNA) fingerprinting.

Results in previous works [1, 3, 4] are MATLAB based ® simulated signals [1] using the QMFB process to evaluate frequency modulated CW (FMCW) and binary phase shift keying (BPSK) signals. Additional work has been done with laboratory based

signals [4] using the QMFB process to evaluate noise technology radar (NTR) signals.

The 802.11a Wi-Fi and 802.16e WiMAX RF communication protocols [9, 12] are continuously evolving to provide greater reliability using orthogonal frequency division multiplexing (OFDM) techniques to better exploit available communication channel resources. Besides the synchronization and other preset component features, these signals present a wideband noise-like behavior. This is a result of random symbol assignment making detection using burst integration methods more difficult. This provides the motivation to check if QMFB processing is applicable to experimental OFDM-based signals, like 802.11a Wi-Fi and 802.16e WiMAX, with an aim to determining if useful information exists in QMFB output response that relates to specific signal features.

1.1.2 Technical Motivation

The technical motivation is aimed at presenting a new approach for signal exploitation of OFDM-based signals. These signals were chosen because of their noise-like behavior, and specifically the 802.11a Wi-Fi and 802.16e WiMAX signals because of the randomness within signal generation.

The QMFB process is the baseline for conducting this research and when implemented according to its definition [1, 3, 4] has demonstrated a consistent approach to estimating signal parameters such as bandwidth (W), center frequency (f_c), signal duration (T_s), modulation type (AM, FM, BPSK, QAM, etc), frequency content and time allocation.

In this research the signal structure for each protocol, specifically the signals'

physical layer, contains details related to transmitted signal characteristics, and those details define what the received signal structure should be. By exploiting the QMFB process using an OFDM-based signal input, the goal is to realize the extent that signal characteristics can be reliably extracted and how well the extracted features match the defined structure [9, 12].

1.2 Research Objectives

The main objective for this research is to perform a qualitative visual assessment of OFDM-based signal responses using passive QMFB detection. This objective was divided in two parts, including: 1) reducing the required computation time used in previous works [1, 3, 4] to perform QMFB processing, and 2) improving output results related to frequency and time resolution for a given signal of interest. The goal is to achieve frequency and time resolution that permits reliable visual assessment to enable exploitation of a given signal's characteristics from an operator's perspective within an reduced computation time. This empirical approach would permit exploitation of signal characteristics such as bandwidth (W), center frequency (f_c), signal duration (T_s), frequency content and time allocation as presented in 2D QMFB F-T plots.

1.3 Research Organization

The document includes general descriptions and information for specific cases that were used to compute the results according to the research objectives defined in previous section.

Chapter 2 presents the necessary technical background used as a baseline during this research effort. Description about QMFB process is presented along with an OFDM

overview and some basic characteristics of the signals of interest with emphasis on physical layer characteristics [9, 12].

Chapter 3 presents the adopted methodology aimed to compute the necessary results to achieve the defined objectives according to the technical background defined in previous chapter. A process overview is presented and its decomposition is described. The post-collection process is defined first, followed by verification and validation of the QMFB process. The input signal parameters are then verified according to the standards defined for each case [9, 12]. The QMFB process is described, including the effects of signal resampling and zero-padding used for given input signals. Measurable process outputs are defined, signal of interest parameters are provided, and the graphical presentation format for QMFB results is introduced.

Chapter 4 presents computed simulation results according to the given methodology and comparisons to initial parameters for each signal of interest are presented. Initial conclusions for each case are also presented. The results are presented in 2D F-T plots along with corresponding 1D plots for time domain and frequency domain responses. Overlay plots are used for initial input signal, output signal and burst integrated output signal comparisons.

Chapter 5 presents the research summary and conclusion. The motivation, methodology and computed versus expected results are discussed. Recommendations for future work are given. Finally, appendices are provided for each signal of interest along with the implemented MATLAB® code.

CHAPTER 2.

Background

2.1 Overview

This chapter provides the technical background established for this research effort. This chapter is divided in two main sections aimed at defining a performance baseline and providing basic concepts related to the topics and experimental techniques exploited during this research. The Quadrature Mirror Filter Bank (QMFB) process is described in Section 2.2, which provides general implementation parameters and assumptions. Fundamentals of Orthogonal Frequency Division Multiplexing (OFDM) are introduced in Section 2.3 which provides the general signal structure as well as key signal features. There were two OFDM-based signals of interest for this research. The physical layer characteristics of each are provided in Section 2.4 for the 802.11a Wi-Fi signal and Section 2.5 for the 802.16e WiMAX signal.

2.2 Quadrature Mirror Filter Bank (QMFB) Processing

The QMFB is an orthogonal waveform decomposition technique based on wavelet filter theory. Each layer output provides input signal frequency and time characteristics aimed to estimate and exploit various signal's features. Common features of interest include signal modulation type, bandwidth, frequency component distribution, signal duration as well as time and frequency allocation. As detailed in Figure 2.1, the process adopted here was introduced by Pace [1] and subsequently exploited in additional related works of Jarpa and Atienza [3, 4]. Jarpa's research in [3] was based on verifying QMFB response given structured signal inputs, including a single tone, multiple tone,

frequency modulated continuous wave (FMCW), and frequency/phase shift keyed (FSK/PSK) waveforms. Atienza's research in [3, 4] analyzed the QMFB response given noise-like input signals collected from AFIT's Noise Technology Radar (NTR) Noise Network (NoNET).

For a given input signal, the QMFB process performs waveform decomposition by computing continuous signal decimation in high and lower frequency components using the signal structure detailed in Figure 2.1. The input signal is decomposed into in-phase (I) and quadrature (Q) components using modified sinc-shaped filters [1].

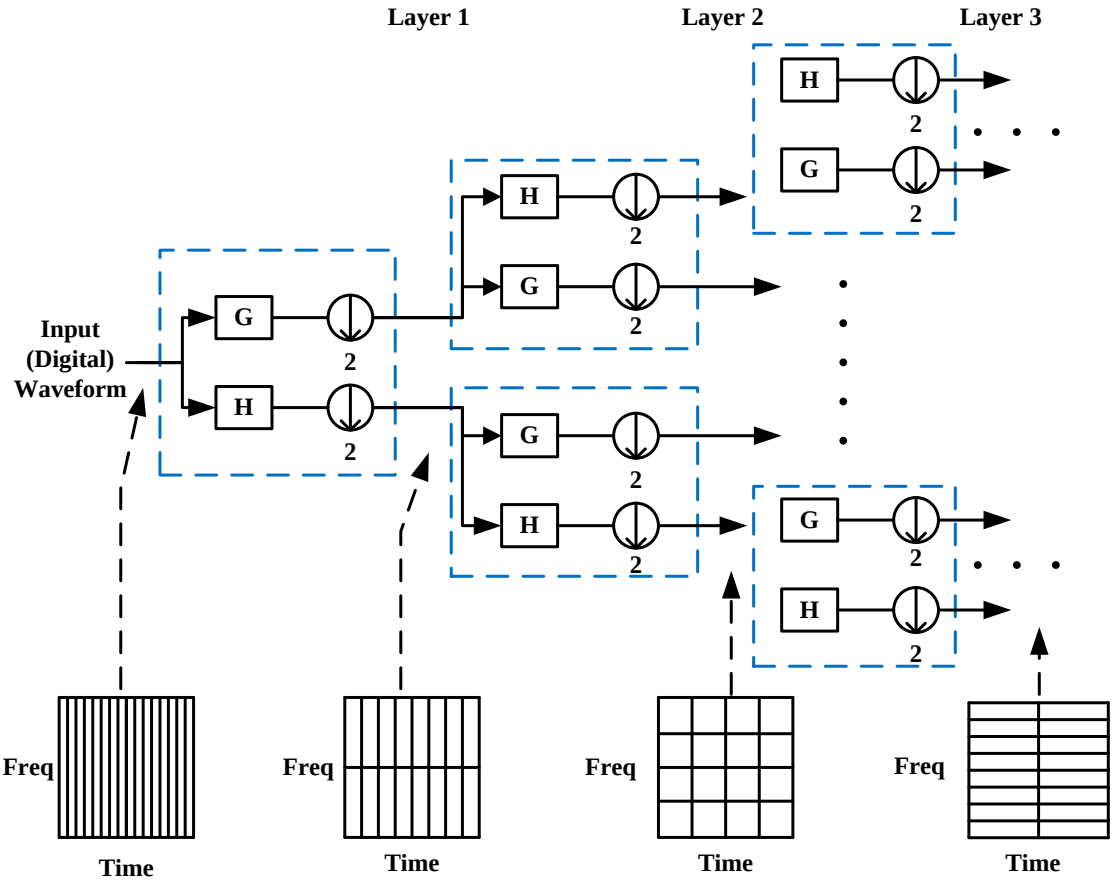

Figure 2.1 QMFB process overview [1]

The output of each filter "Layer" corresponds to the amplitude (real or complex) or magnitude as a function Frequency-Time (F-T) parameters according to the input signal. After each filtering stage, the signal is decimated so further layers can be computed. Because of the decimation process, and the filter input signal being a function of the previous layer, the initial time window (duration) is increased by a power of two with every computation. On the other hand, the initial frequency window (bandwidth) decreases according to the same power of two. This creates a tradeoff between the different layers which could produce useful data for a given layer. Given the post-filtering decimation, the total numbers of available layers (N) is a function of the initial number of data samples (N_s) and given by:

$$N=log_2(N_s) \tag{2.1}$$

For a given N, the frequency window extent (Δf) and time window duration (Δt) for a given layer (N_L) can be computed as follows:

$$\Delta f = \frac{f_s}{2(2^{N-1}-1)} = \frac{f_s}{N_F} \tag{2.2}$$

$$\Delta t = \frac{2^N}{f_s(2^{N-1}-1)} = \frac{2^N}{f_s N_T} \tag{2.3}$$

Where f_s is the sampling frequency, N_F is a given frequency layer number, and N_T is a given time layer number. According to (2.2) and (2.3) it can be seen that lower numbered layers present shorter time windows compared to higher layers and there is an inverse relationship with the frequency window.

The decimation is computed according to [1], which was proven to work in

previous works [3, 4] and it consist in the implementation of a “modified sinc” finite impulse response (FIR) given by:

$$h[n]=\sqrt{\frac{S}{2}}sinc\left(\frac{n+0.5}{C}\right)w[n], \quad -\frac{N}{2}\leq n \leq \frac{(N-2)}{2}, \tag{2.4}$$

Where S is the scaling variable, C is the compression variable, N is the number of coefficients, and $w[n]$ is a Hamming window weighting.

These particular filters have a flat bandpass response and pass the maximum amount of desired signal energy at each layer. According to [1, 3] with an aim of getting “nearly orthogonal filters with cross-correlation of less than 0.001” using $N = 512$, the constant compression and scaling values in (2.4) are C=1.99375872338059 and S=1.00618488680080. The Hamming window is use to suppress the effects of Gibb’s phenomena resulting from sequence truncation [1, 3].

To avoid data sample loss, and because the total number of available layers is given by (2.1), the following assumption has been made to compute, as initial approximation, the total number of available layers for a given input signal:

$$N=ceil[log_2(N_s)] \tag{2.5}$$

Where N is the total number of available layer, N_s is the number of samples, and the ceil[ ] operation ensures zero-padding to the next power of two.

2.3 Orthogonal Frequency Division Multiplexing (OFDM) signals

The sub-carrier frequencies in OFDM are chosen to be mutually orthogonal and inter-carrier guard bands are not required as in basic modulation process. This simplifies the transmitter and receiver designs; unlike conventional FDM, which requires a separate

filter for each sub-channel.

Considering the frequency domain, an OFDM symbol is made up multiple subcarriers, the number of which determines the Fast Fourier Transform (FFT) size used. As illustrated in Figure 2.2 [12] there are three distinct types of subcarriers used. The type of subcarrier and purpose are as follows:

- Data Subcarriers: Data Transmission
- Pilot Subcarriers: Signal Estimation
- Null Carriers: No transmission; guard bands and DC subcarrier.

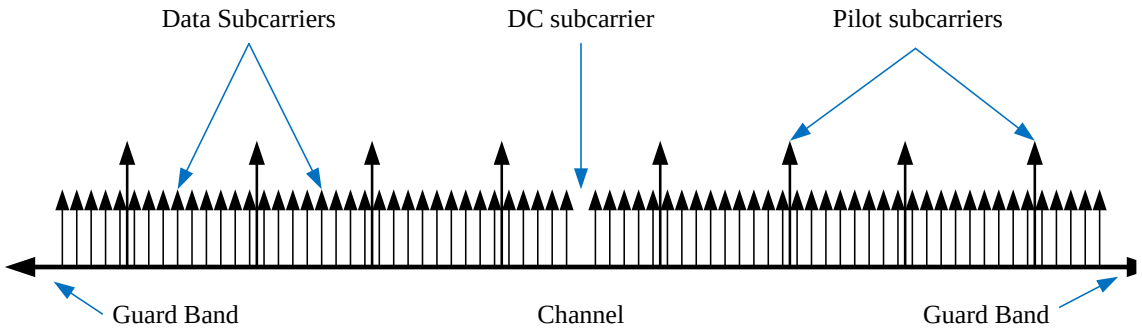

Figure 2.2 OFDM frequency structure [12]

Considering time domain, an Inverse Fourier Transform (IFT) creates the OFDM waveform where the signal time duration (T_s) is the result of the initial Guard Time (T_g) plus the useful symbol time (T_b). A T_g copy of the last useful symbol is added and used to correct for multipath. Therefore, the basic OFDM time structure is given by Figure 2.3.

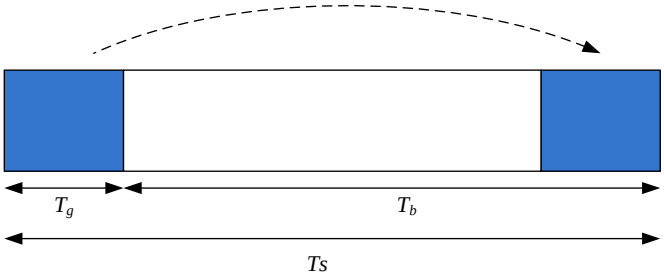

Figure 2.3 OFDM time structure [12]

The resultant transmitted signal is given by

$$s(t)= Re\left(e^{j2\pi f_c t} \sum_{k=\frac{-N_{used}}{2},\, k\neq 0}^{\frac{N_{used}}{2}} c_k e^{j2\pi k\Delta f(t-T_g)} \right) \tag{2.6}$$

Where f_c is the center carrier frequency, N_{used} is the number of used subcarriers, c_k is a complex modulation number specifying a point in the QAM signaling constellation, Δf is the subcarrier spacing, t is the elapsed time since the beginning of the OFDM symbol, and $T_g = G \times T_b$ with defined $G \in [1/4, 1/8, 1/16, 1/32]$ [12].

According to the OFDM frequency and time definitions given above, an OFDM-based signal is generated as given by Figure 2.4

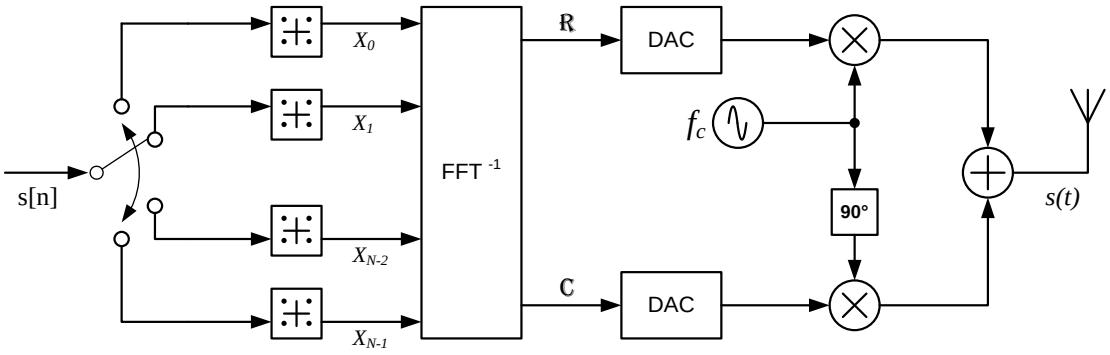

Figure 2.4 OFDM-Based Signal Generation Process

2.3.1 OFDM-Based 802.11a Wi-Fi Signal

This OFDM-based signal is widely used in the implementation of wireless local area networks (WLAN). According to [9] and related to this research effort, the OFDM 802.11a signal covers the following frequencies 5.15–5.25 GHz, 5.25–5.35 GHz, and 5.725–5.825 GHz. This provides a wireless LAN with data payload communication bit rates of $R_b \in [6, 9, 12, 18, 24, 36, 48, 54]$ Mbit/s. The system uses $N_s = 52$ subcarriers that are modulated using binary phase shift keying (BPSK), quadrature phase shift keying (QPSK) or 16-ary, 64-ary quadrature amplitude modulation (16-QAM or 64-QAM). The defined 802.11a Wi-Fi signal frame format [9] according to the Physical Layer Converge Procedure (PLCP) is defined as the PLCP Protocol Data Unit (PPDU) and includes the OFDM PLCP preamble, OFDM PLCP header and the PLCP service data unit (PSDU) as shown in Figure 2.5.

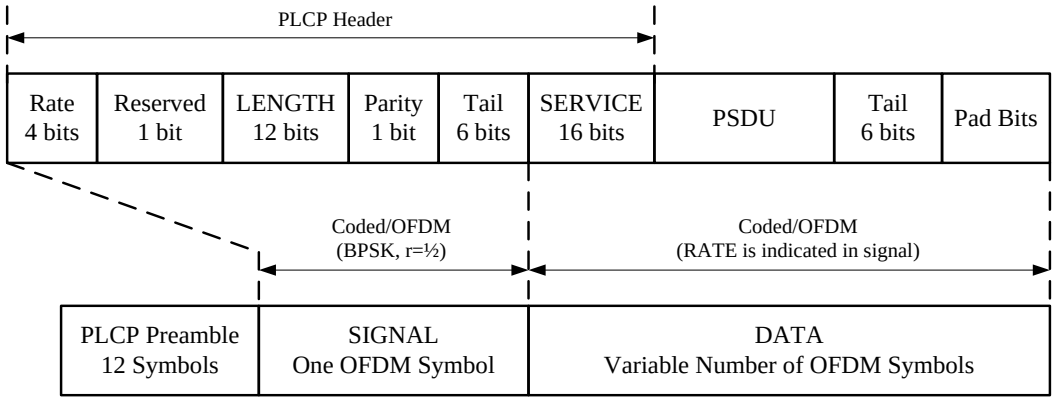

Figure 2.5 PPDU frame format [9]

The PLCP preamble field is present for the receiver to acquire an incoming OFDM signal and synchronize the demodulator. The preamble consists of 12 total symbols, including: 1) ten *short* symbols for establishing automatic gain control (AGC),

coarse carrier frequency estimation, and 2) two *long* symbols for fine frequency acquisition in the receiver. The PLCP preamble structure is shown in Figure 2.6.

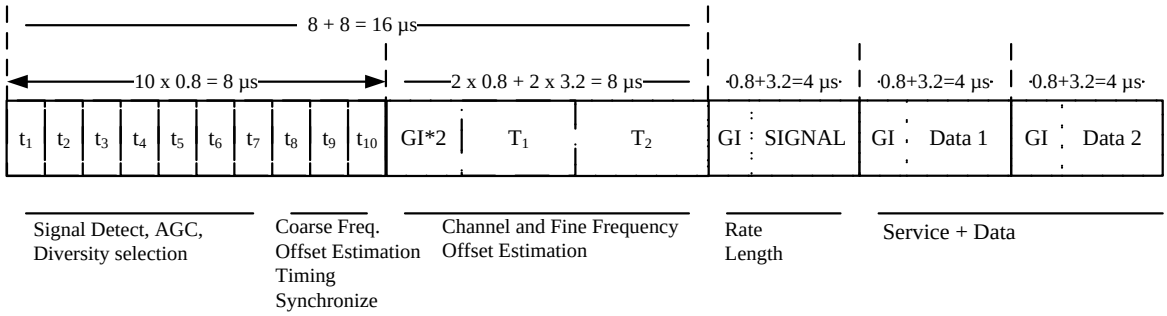

Figure 2.6 802.11a Wi-Fi Signal preamble structure [9]

2.3.2 OFDM-Based 802.16e WiMAX Signal

This protocol is aimed to extend wireless range of previous WLAN protocols and provide broadband connectivity for data and telecommunications. According to [12] and related to this research effort, the OFDM 802.16e signals cover the frequency bands below 11GHz. In this case, each data frame is divided in two subframes, including: 1) the down link (DL) subframe aimed to transmitting data and control messages to specific subscriber station (SS) and 2) the up link (UL) subframe that is used by the subscriber to transmit to the Base Station (BS). Each subframe can be modulated using BPSK, QPSK, 16-QAM or 64-QAM. The defined 802.16e WiMAX Signal frame can be formatted using either time division duplexing (TDD) or frequency division duplexing (FDD) techniques. As shown in Figure 2.7 for TDD, the generic 802.16e WiMAX Signal frame time duration is obtained by adding each subframe (DL and UL) per SS.

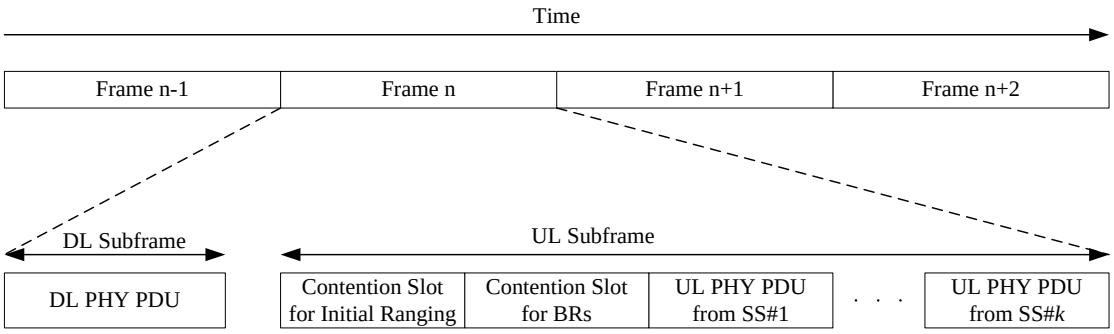

Figure 2.7 OFDM frame structure with TDD [12]

As shown in Figure 2.8 for FDD, the generic 802.16e WiMAX Signal frame time duration is constant. The subframes (DL and UL) for all SSs use the same time frame but with different frequencies.

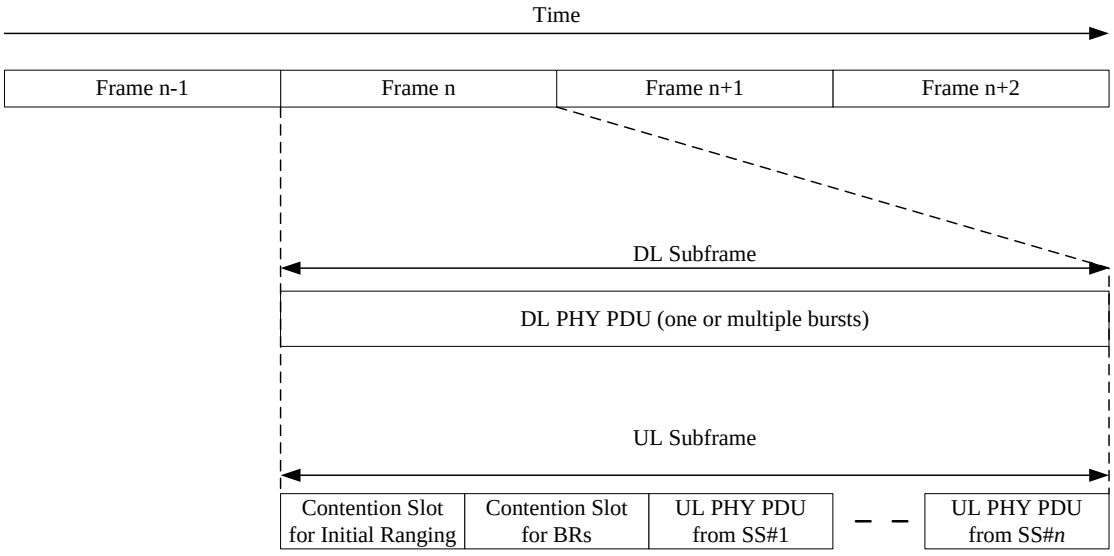

Figure 2.8 OFDM frame structure with FDD [12]

2.4 Summary

Technical background for the research effort has been presented, to include a discussion of the QMBF process and characteristics. The total number of samples, sample frequency and zero padding were described as key parameters aimed to achieve Δf and Δt which allow reliable qualitative visual assessment according to the available generated layers. Fundamentals of OFDM were introduced and two specific OFDM-based signals of interest described. This included a discussion of relevant physical layer characteristics for 802.11a Wi-Fi and 802.16e WiMAX signals.

CHAPTER 3.

Methodology

3.1 Introduction

This chapter discusses the adopted methodology aimed at performing the necessary data and simulation management to satisfy defined objectives in this the research effort. Section 3.2 provides the process overview which shows the main flow diagram that was used as the baseline process for the research effort. Section 3.3 describes the verification and validation (V&V) signals used to ensure the QMFB process was implemented correctly. This is followed by Section 3.4 which describes the OFDM-based signals considered for demonstrating the exploitation capability of the QMFB process. Implementation of the QMFB process is detailed in Section 3.5, to include the effects of signal resampling and zero-padding for a given input signal. Finally, the chapter concludes with Section 3.6, results presentation format, which shows how results are presented for each case considered.

3.2 Process Overview

The flow diagram in Figure 3.1 was developed to set the sequence of steps aimed at achieving the objectives described in Chapter 1 and based on background information given in Chapter 2. The goal was to provide measurable results at every different stage of the modeled problem. For each input, signal characteristics were first verified using both time domain and frequency domain power spectral density (PSD) responses. Once verified, the signal was input to the QMFB process and the resulting layer outputs were used to exploit features. The exploitation assessment included two steps: 1) Seeing how

well resultant QMFB features match the 1-D time and PSD characteristics of the input signal, and then 2) Using qualitative visual assessment to see if the 2-D QMFB F-T outputs provided an additional insight on features not evident in 1-D responses.

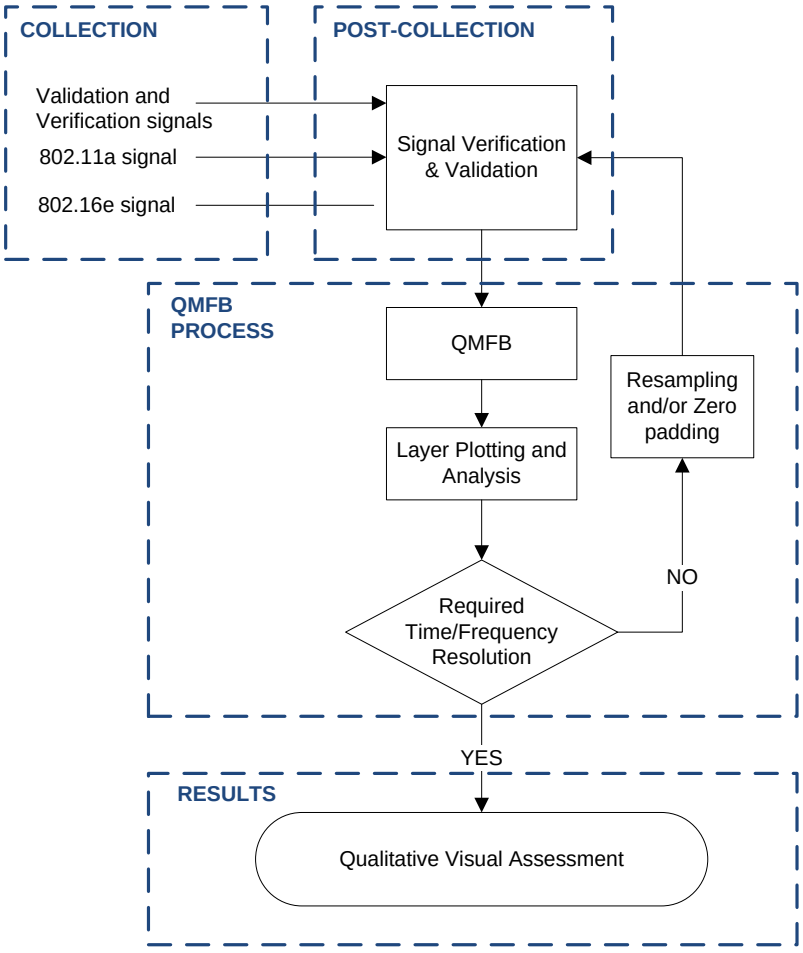

Figure 3.1 Overview of Research Methodology

3.3 Verification and Validation (V&V) signals

To ensure the QMFB process was implemented correctly, QMFB output responses were looked at using two specific input signals for V&V. The two analytic V&V signals included a continuous LFM-modulated signal and a discrete multi-tone

signal used for V&V in previous work [1, 3, 4]. The signal's characteristics presented on each V&V signals are aimed to realize differences on the QMFB response due to continuous modulation, discrete modulation, and single versus multiple frequencies. Signal generation parameters for each of the V&V signal are set to establish identical QMFB processing parameters as provided in Table 3.1

Table 3.1 QMFB Parameters for V&V Signal Processing

Bandwidth (KHz)	Samp Freq f_s (Hz)	Duration (mSec)	Number of Samples
40	100	1.6	2428

3.3.1 Continuous Linear FM (LFM) signal

The LFM V&V signal was used to assess the QMFB response to a continuous signal input having a linear frequency and amplitude change during the signal duration [2]. The signal time and PSD response is shown in Figure 3.2 were generated using the analytic expression in (3.1) with f_L = 45 KHz , f_H = 95KHz, and $f_\Delta = (F_L - F_H) = -50$ KHz.

$$\begin{aligned} s_1(t) &= A_1 \sin(2\pi f_H t) && 0 < t < 0.6\,m \\ s_2(t) &= A_2(t) \sin(2\pi f_\Delta t^2) && 0.6\,m \le t < 1.0\,m \\ s_3(t) &= A_3 \sin(2\pi f_L t) && 1.0\,m \le t < 1.6\,m \end{aligned} \qquad (3.1)$$

$$s_{LFM}(t) = \sum_{i=1}^{3} s_i(t)$$

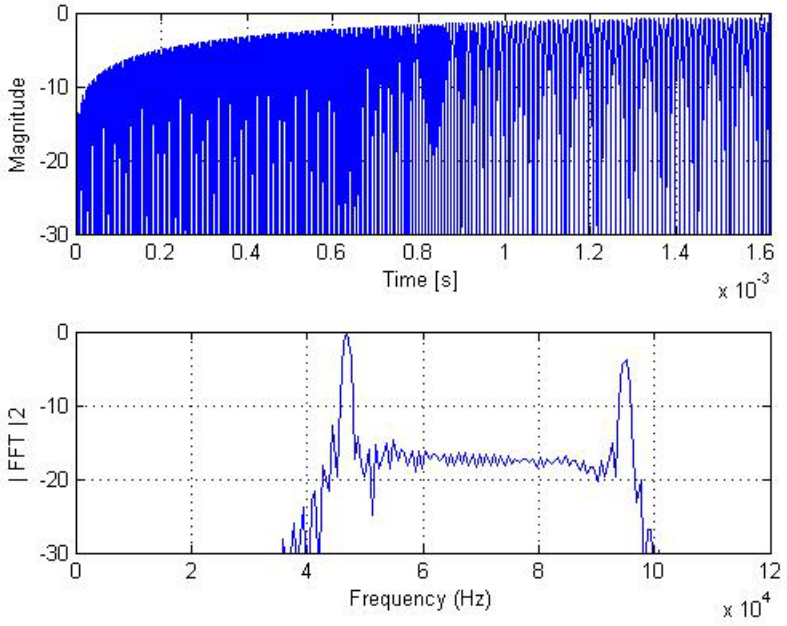

Figure 3.2 Analytic LFM V&V signal time domain and PSD responses.

3.3.2 Discrete Multi-Tone (DMT) V&V Signal

The DMT V&V signal was generated consistent with Szmajda's V&V signal in [7] and was chosen to assess the QMFB response to a discrete modulated signal having both single and multiple frequency components across time. The signal time and PSD responses are shown in Figure 3.3 and were generated using the analytic expressions in (3.2) and tone parameters provided in Table 3.2

$$
\begin{aligned}
s_1(t) &= A_1 \sin(2\pi f_1 t) && 0 < t < 13 \\
s_2(t) &= A_2 \sin(2\pi f_2 t) && 13 < t < 25 \\
s_3(t) &= 0 && 25 < t < 37 \\
s_4(t) &= s_1(t) && 37 < t < 50 \\
s_5(t) &= A_5 \sin(2\pi f_5 t) && 37 < t < 50 \\
s_6(t) &= A_6 \sin(2\pi f_6 t) && 37 < t < 50
\end{aligned}
\tag{3.2}
$$

$$
s_{DMT}(t) = \sum_{i=1}^{6} s_i(t)
$$

Table 3.2 Discrete Multi-Tone Szmajda Signal Generation Parameters

Tone	$s_1(t)$	$s_2(t)$	$s_4(t)$	$s_5(t)$	$s_6(t)$
Amplitude	$230\sqrt{2}$	$2A_1$	A_1	A_1	A_1
Frequency (Hz)	5	5	5	10	40

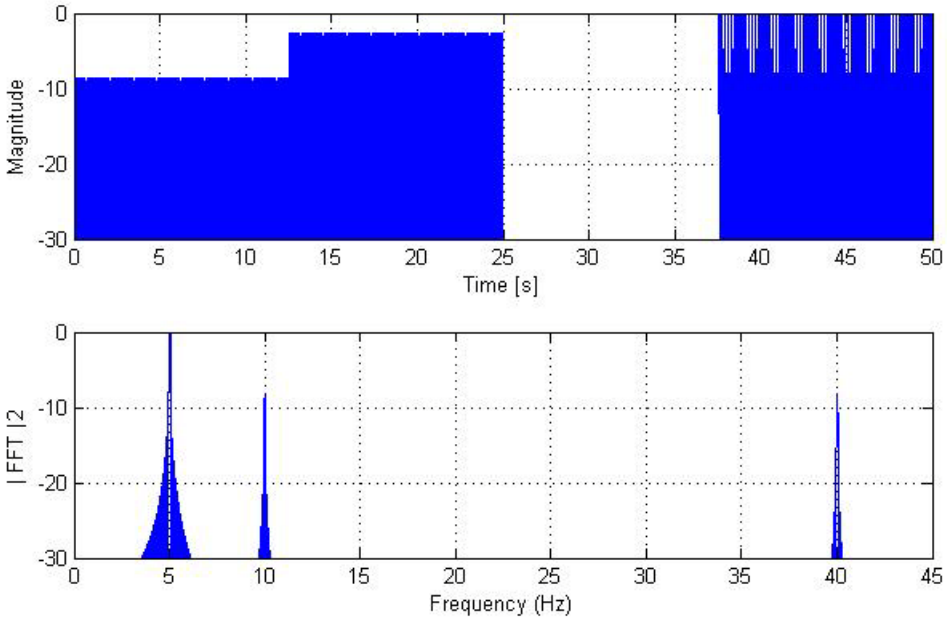

Figure 3.3 Analytic DMT Szmajda V&V signal time domain and frequency responses.

3.4 OFDM-Based Signals

The QMFB response to the V&V signals described in Section 3.2 and Section 3.3 provide a baseline for assessing QMFB exploitation potential using two OFDM-based signals. Each signal was decomposed according to its specific characteristics in order to find, evaluate and exploit different responses. The two signals considered include experimentally collected 802.11a Wi-Fi [8] and 802.16e WiMAX [0, 11] signals.

3.4.1 802.11a Wi-Fi signal

This OFDM signal was chosen because of its well-known and structured physical layer response as described in Chapter 2. In this case, the signal used corresponds to experimental collections taken to support results in [8]. The signal was analyzed in three stages using 1) an isolated preamble response, 2) a single burst response and 3) an integrated burst response.

During the first analysis stage the 802.11a preamble response was isolated and only the first 10 short symbols corresponding to the first half of the preamble was considered. During the second analysis stage, the response of a single 802.11a burst was set as input to the QMFB process. Finally, burst integration was computed considering the mean amplitude response for $N_B = 500$ burst collections. The 802.11a Wi-Fi signal parameters for each analysis case are presented in Table 3.3

Table 3.3 802.11a Wi-Fi Signal Parameters

Input	Bandwidth (MHz)	Samp Freq f_s (MHz)	Duration (μSec)	Number of Samples
Preamble	8.0	23.75	135	3200
Burst	9.0	23.75	124	2945

3.4.2 802.16e WiMAX signal

This signal was chosen to assess the QMFB response using a more complex structured OFDM-based signal input. In this case, the input signal corresponds to experimental collections made in support of work in [0, 11]. The process is aimed to exploit the physical layer parameters and structure described in Chapter 2 according to [12]. The experimental 802.16e WiMAX signal was analyzed in two stages. First, the

range-only mode response was considered as input for two cases, including single burst and burst integration using $N_B \approx 1400$ bursts. Secondly, the *data-only* mode response was considered as input for two cases, including single burst and burst integration using $N_B \approx 640$ bursts. The 802.16e WiMAX signal parameters for each case described above are presented in Table 3.4

Table 3.4 802.16e WiMAX Signal Parameters

Mode	Bandwidth (MHz)	Samp Freq f_s (MHz)	Duration (mSec)	Number of Samples
Range-Only	2.0	11.875	0.381	4521
Data-Only	2.5	11.875	1.61	19125

3.5 QMFB Processing

Aimed to evaluate experimental results according to the available inputs described in Section 3.3 and Section 3.4, the QMFB process was first modeled in MATLAB® based on previous work [1, 3, 4] and according to the process described in Chapter 2. The length of each input signal vector was first checked and zero-padded to the closest integer power of 2 to avoid data loss during QMFB processing (2.5). Then, the first simulation trial was completed. After verifying that the QMFB process was working for every available input signal type, multiple trials were completed to check differences and to choose the best QMFB layer output response according to the specific input. According to the available data format for a given input, up to four different cases were used in the modeled QMFB process. The initial simulation parameters used to check QMFB performance are shown in Table 3.5

Table 3.5. Initial QMFB Configuration

Input	Real (R), Complex(C), Magnitude
# Filter Coefficients	512
Window	Hamming
f_s	Initial Sample Frequency
Total # QMFB Layers	Ceil{$\log_2$[length(input)]}

Given an input vector to the QMFB process, the first "Layer" output is computed, decimated, stored, and passed to the next layer. This iterative process repeats and ends after the initial vector is decimated according to:

$$N_L = log_2(Data\ Length) = \text{Total \# Available Layers} \tag{3.3}$$

Because data length is a function of both sampling frequency (f_s) and total signal duration (T_s), two pre-conditioning steps were included in the QMFB process, henceforth referred to as resampling and zero-padding. Thus, each input signal was resampled, zero-padded and set as input to the QMFB process to achieve the desired frequency and time resolution in a given QMFB layer output. According to the QMFB frequency-time tradeoff described in Chapter 2, better time resolution is achieved in lower QMFB layers, but better frequency resolution is achieved in higher QMFB layers. So the challenge is to find a frequency sampling rate *(f_s)* versus signal duration *(T_s)* aimed to present an accurate representation of input signal characteristics. Henceforth, this is called the "*the most representative layer"* which corresponds to the layer which shows frequency and signal time allocation that could be useful to exploit input signal features such as signal bandwidth (*W)*, signal duration *(T_s)*, time resolution (Δt) and frequency resolution (Δf). Figure 3.4 shows a collection of QMFB outputs where "*the most representative layer"* corresponds to layer #20 (Q_{20}) highlighted in the red dashed rectangle.

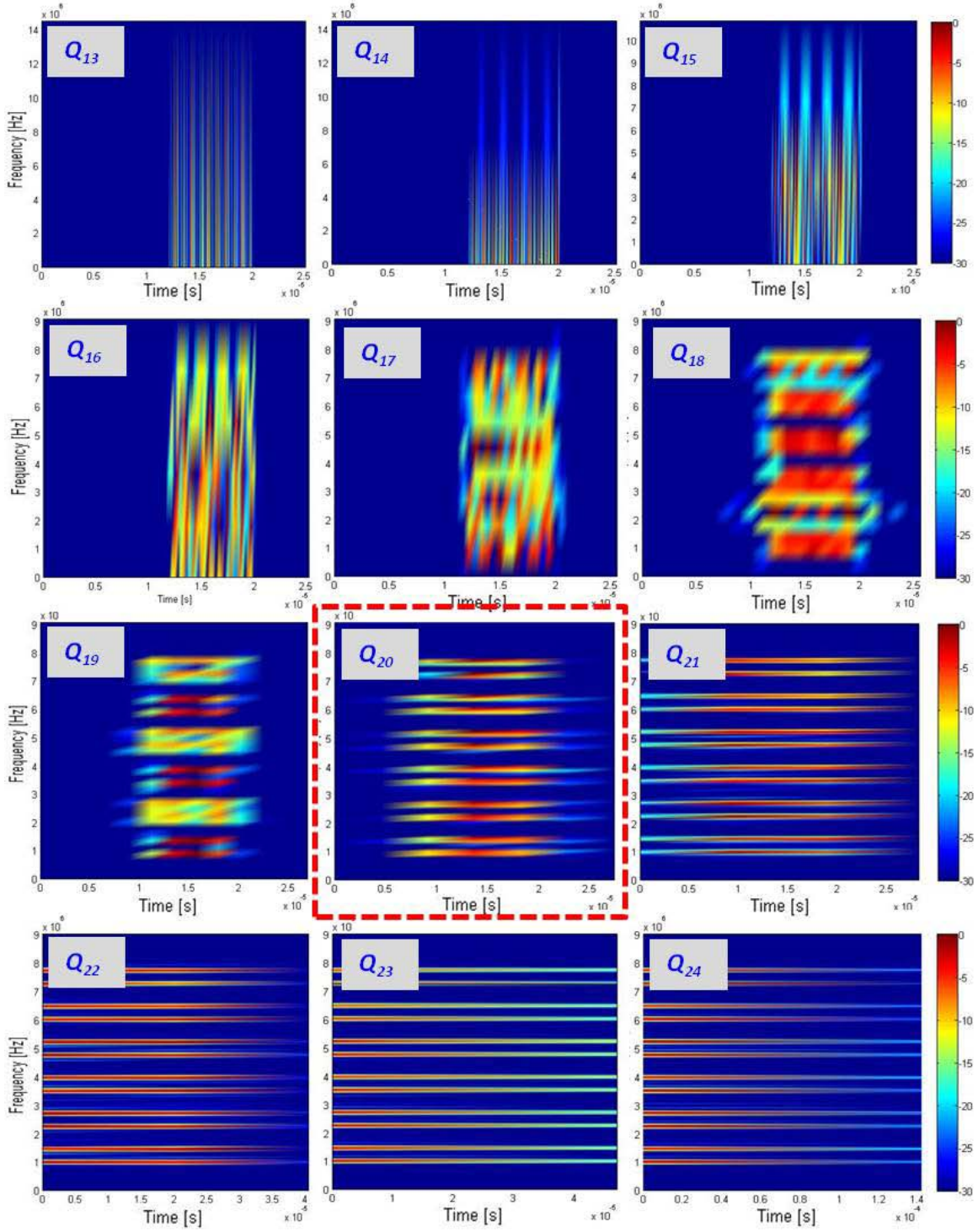

Figure 3.4 QMFB output collection sample

3.5.1 Signal Resampling

By resampling the input signal, the number of available input data samples increases without changing the total signal duration T_s. This also increases the effective sampling frequency f_s and because of the F-T trade-off in QMFB processing, it is expected that "*the most representative layer*" should be located in upper layers, which increases required computing time and time resolution Δt for a given input signal.

3.5.2 Zero Padding

By zero-padding the input signal, the total effective time duration T_s is increased, so better frequency resolution is achieved for a given signal and it is expected that the *most representative layer* is now located in lower layers. But lower layers present poorer signal frequency resolution (increased Δf), therefore by using lower layer analysis results could be an inaccurate signal representation.

3.5.3 Measurable outputs

Aimed to extract useful data and to reduce computation time of the QMFB process, the QMFB process was divided in four steps, named as: 1) *layer generation minimization,* 2) Q_N *matrix formatting,* 3) *time analysis* and 4) *frequency analysis*. By performing *Layer Generation Minimization* it was possible to reduce the total number of generated layers, because higher layers does not improve qualitative visual analysis and can be disregarded. The Q_N *matrix formatting* is a matrix dimensional reduction aimed to disregard irrelevant analysis data such as induced by zero-padding and high frequency data falling outside the processed bandwidth of the input signal. In this case, the first useful plots can be computed considering three variables, including 1) desired layer

number, 2) upper frequency limit, and 3) upper time limit. The resultant output *Q_n.mat* file was created (were *n* denotes a given layer number) considering an amplitude (real or complex) matrix, a magnitude matrix, Δt and Δf values for a given layer, time vector, frequency vector and f_s. The *time analysis* and *frequency analysis* steps permit comparison of input data and QMFB responses in order to realize process accuracy and losses due to the signal processing. Figure 3.5 shows all the available measurable outputs and their relation to the QMFB computing process.

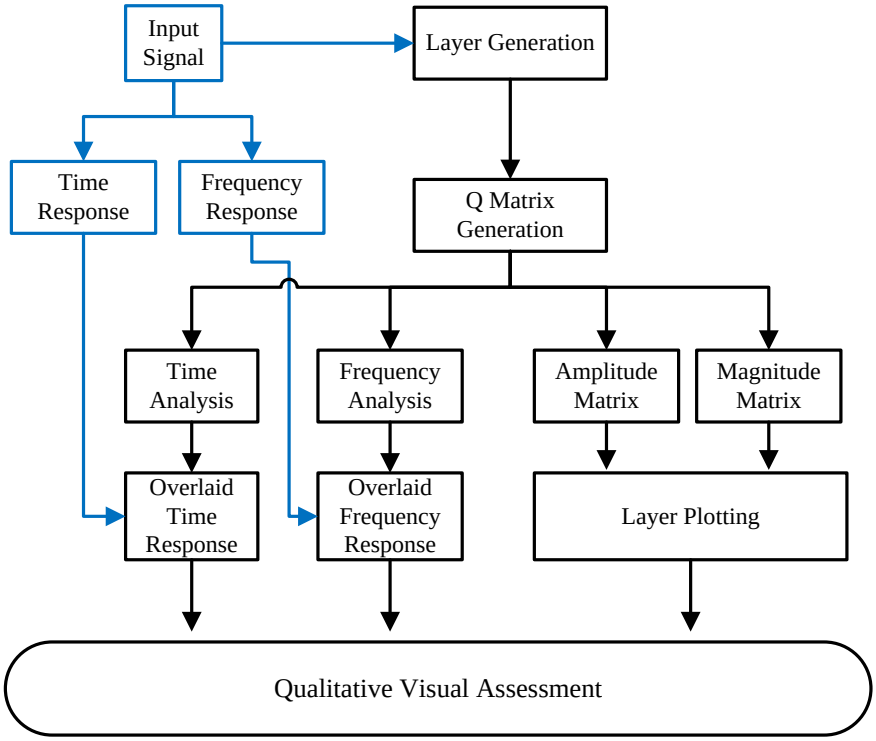

Figure 3.5 Measurable process outputs

3.5.4 Presentation of QMFB Layer Outputs

Aimed to the objective of providing QMFB qualitative visual assessment, the results are presented in frequency versus time (F-T) plots for "*the most representative layer*" along with the average frequency and average time plot of the input processed

signal. The QMFB layer output data can be presented in many formats. For clarity and to enable consistent comparison as the input signal varies, all results presented in Chapter 4 use the format presented in Figure 3.6 which includes numbered responses of:

1. The normalized average frequency response computed as a *row-wise* average for a given QMFB layer data.
2. *"The most representative layer"*, corresponds to a 2D QMFB F-T layer output plotted using Matlab® *pcolor* function followed by *shading interp.* Appendix B contains a complete set of 2D F-T for given signal.
3. The normalized average time response computed as a *column-wise* average for a given QMFB layer data.

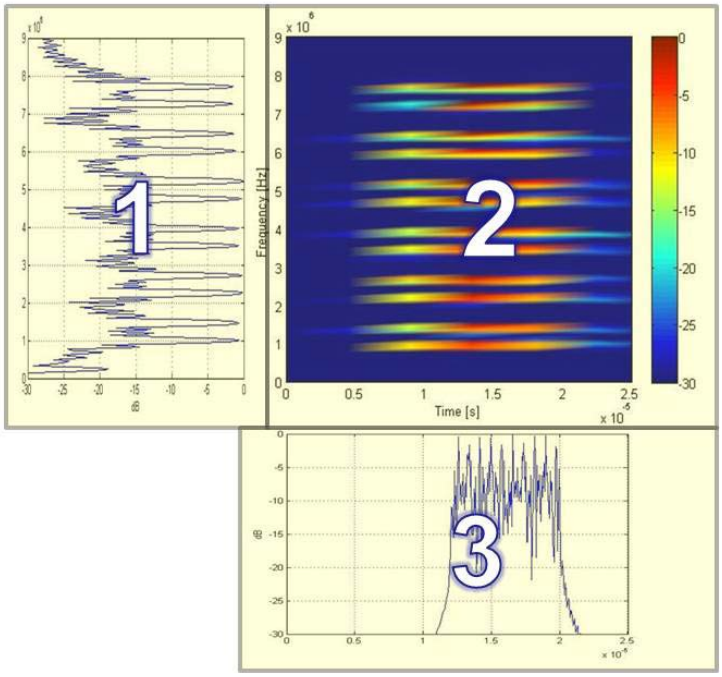

Figure 3.6. Representative Presentation Layout for a given QMFB layer output showing (1) 1-D *Average Frequency*, (2) 2-D *QMFB*, and 1-D *Average Time* responses

Note: For Chapter 4 results, the plots correspond to three different QMFB layers identified as the most representative responses for a given domain.

3.5.5 Single Burst vs. Integrated Bursts Overlay Plots

Aimed to check QMFB response related to a given signal input, average plots for both time (Figure 3.7) and PSD (Figure 3.8) responses are provided to assess process accuracy and signal processing loses. The following two plots are representative of the presentation format used in Chapter 4.

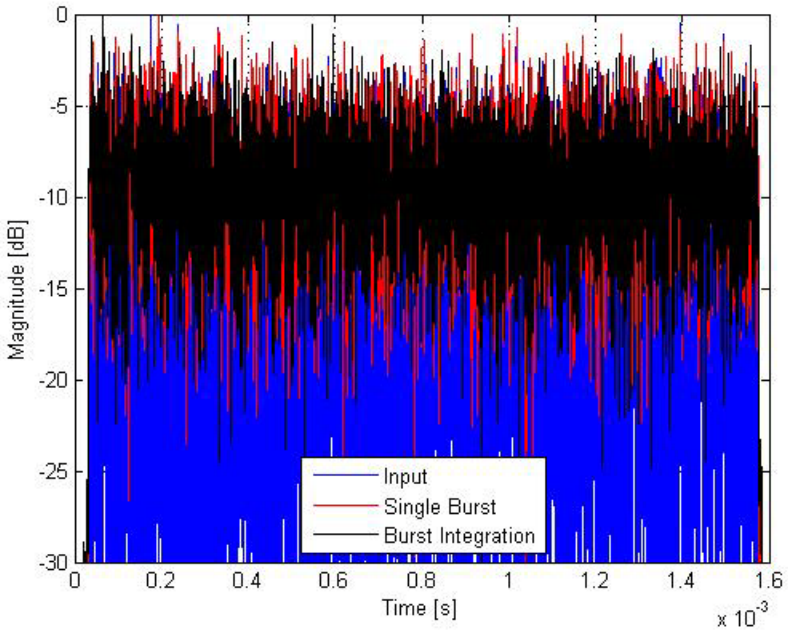

Figure 3.7 Overlay *Time* responses showing input signal response, QMFB output for single and integrated burst

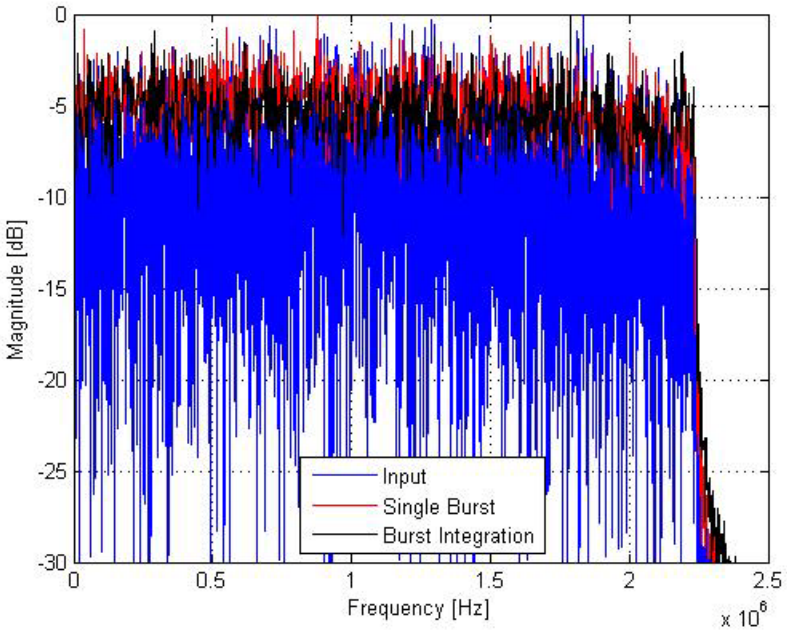

Figure 3.8 Overlay *Frequency* responses showing input signal response, QMFB output for single and integrated burst

3.6 Summary

The methodology presented in this chapter was applied to each of the described input signals. To reduce computation time, the QMFB process was decomposed and measurable outputs at each stage were defined. Using the designed process flow diagram in Figure 3.5, different layers output data are generated, saved and analyzed using qualitative visual assessment to characterize QMFB potential for exploiting unknown signals. The effectiveness of this method is based on signal parameters such as the resampling vector, zero-padding factor, total signal duration, time resolution Δt and frequency resolution Δf for each computed QMFB layer.

CHAPTER 4.

Simulation Results and Analysis

4.1 Introduction

This chapter presents MATLAB® simulation results and data analysis based on that was obtained using the methodology discussed in Chapter 3. Baseline verification and validation (V&V) performance of the QMFB process is first addressed in Section 4.2 using the LFM and analytic Szmajda signals described in Chapter 2. Then, OFDM based signals described in Chapter 2 are input to the QMFB process to determine if visually discernible features are present for estimating signal parameters. The QMFB results are presented in frequency versus time (F-T) plots for a given layer previously defined in chapter 3 as *"the most representative layer"*, along with individual average time and frequency responses. Finally, overlaid plots are presented to compare QMFB process outputs for single burst and integrated burst responses.

4.2 Process V&V Signals

Performance assessment is first performed with the LFM and analytic Szmajda signals described in Chapter 2 input to the QMFB process. QMFB performance is characterized trough *qualitative visual assessment* using joint 2D F-T responses as well as independent 1D frequency and time responses.

4.2.1 LFM-Based V&V Signal

The normalized time and frequency responses for the input LFM-based signal are presented in Figure 4.1. The signal was resampled and zero-padded prior to QMFB processing according to the values shown in Table 4.1. The LFM signal time response

shows that higher frequencies are located in the first half of the signal, after those lower frequency responses are present. Related to the PSD response, it can be seen that the W_{-30dB} bandwidth is located within the $f = 40$ KHz to $f = 100$ KHz range. Two frequencies, $f = 45$ KHz and $f = 95$ KHz, are present with higher power levels of $P = 0$ dB and $P = -4$ dB, respectively. For the rest of the frequencies between the two power peaks it can be seen that there is an inverse relationship between the frequency and signal power, with power decreasing from $P = -16$ dB to $P = -19$ dB.

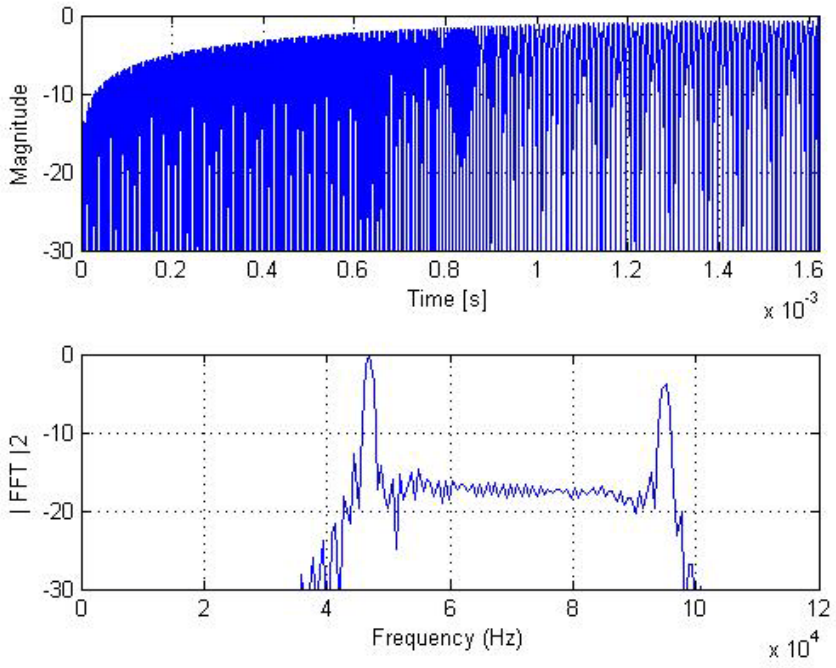

Figure 4.1 LFM V&V signal time domain and PSD responses.

Table 4.1 LFM V&V Signal Parameters

Input	Bandwidth (Hz)	Samp Freq f_s (Hz)	Duration (Sec)	Number of Samples	Sample Rate	Zero Padding
Original	6.0×10^4	1.5×10^8	1.62×10^{-3}	2428	1	N/A
Resampled	6.0×10^4	1.2×10^{11}	3.50×10^{-3}	1942400	800	2^{22}

After pre-processing the LFM signal according to parameters in Table 4.1, the signal was input to the QMFB process. Representative QMFB results for Layer #14 are presented in Figure 4.2 with the signal's linear frequency behavior highlighted (yellow arrows) and power distributed according to color bar. The estimated frequency and time resolution parameters were computed from the F-T plot in Figure 4.2 as $\Delta f \approx 36.62$ KHz and $\Delta t \approx 1.36 \text{x} 10^{-5}$ s. It can be seen that the signal frequency starts and remains at $f = 95$ KHz until $t = 0.65$ *m*s, at which time the frequency decreases linearly to $t = 1$ *m*s. At $t = 1$ *m*s the frequency is $f = 45$ KHz which remains constant until the end of the signal. It also can be seen that the peak signal power is higher in the lower frequency of $f = 45$ KHz and for $f = 95$ KHz the average power is approximately -3.0 dB compared to the maximum signal power. By comparison with analytic signal responses shown in Figure 4.1, the QMFB frequency and time averages show that the process, with some degradation and signal processing loses due to the computing processing and the instant changes of signal frequency, are consistent.

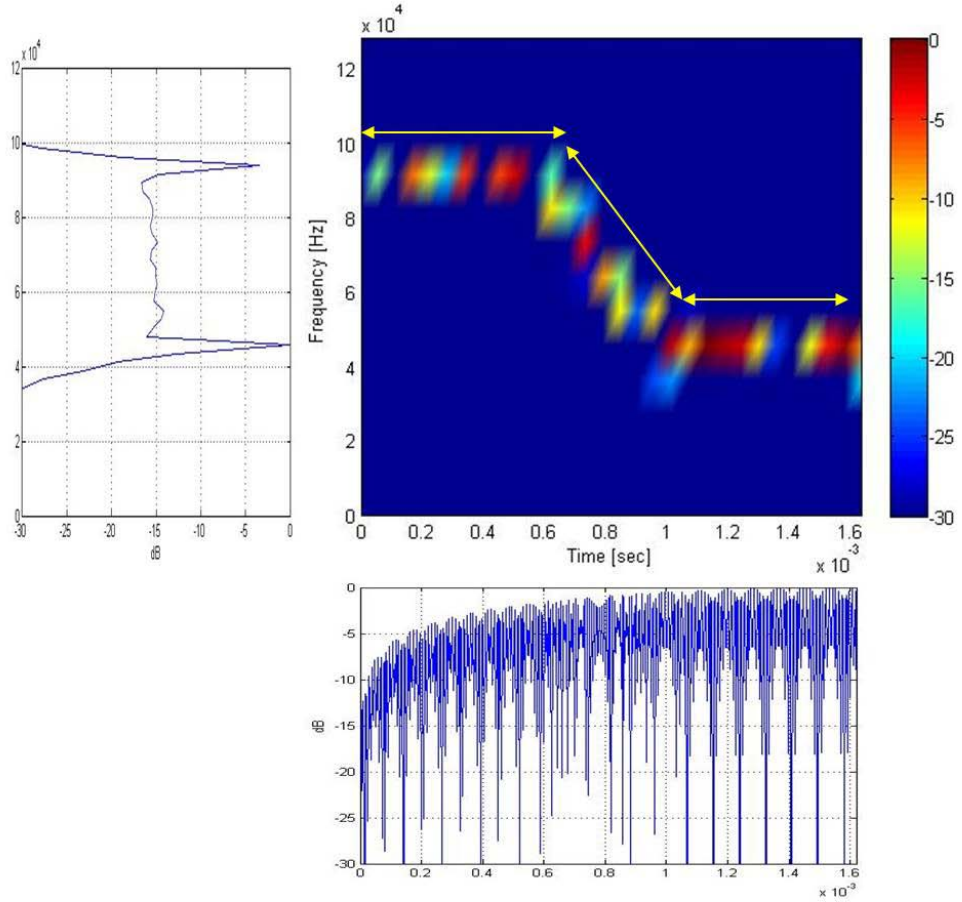

Figure 4.2. QMFB Layer #14 output for LFM V&V signal. Average PSD plot based on Layer #14 as presented and average time plot based on Layer #10.

4.2.2 Analytic Szmajda V&V Signal

The normalized time and frequency responses for the analytic Szmajda signal are presented in Figure 4.3. The signal was resampled and zero-padded prior to QMFB processing according to the values shown in Table 4.2. Related to the time response, four different signal magnitudes can be seen. Besides the absence of a signal response in the $t = 25$ s to $t = 37$ s interval, no other noticeable parameters can be identified. Related to the PSD response, it can be seen that considering the W_{-30dB} bandwidth, three carrier frequencies are present, including $f_c = 5$ Hz, $f_c = 10$ Hz and $f_c = 40$ Hz. The signal

component located at $f_c = 5$ Hz contains the higher power of ($P = 0$ dB) compared to the equal power components located at $f_c = 10$ Hz and $f_c = 40$ Hz ($P = -8$ dB, each).

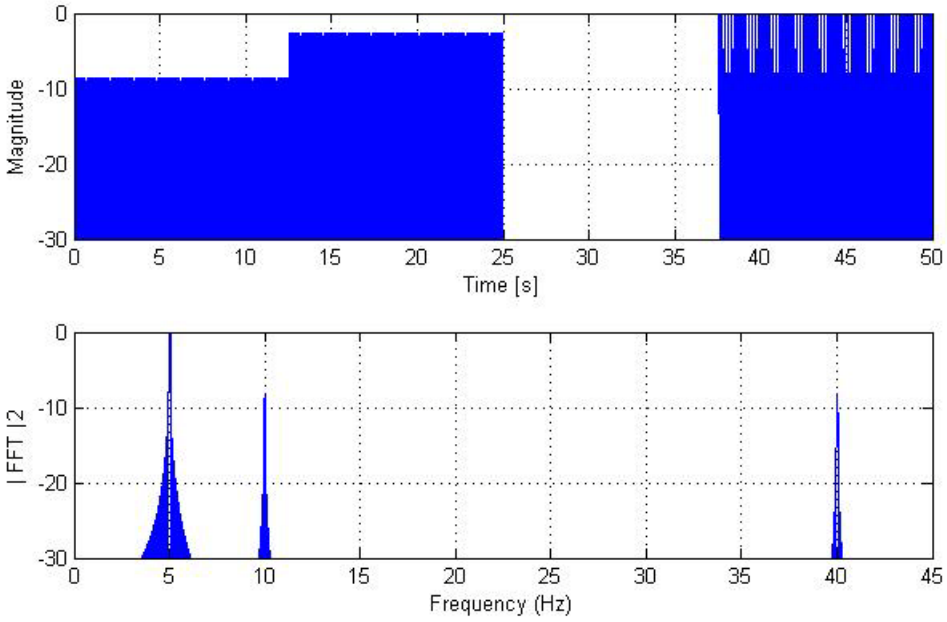

Figure 4.3 Szmajda V&V signal time domain and frequency responses

Table 4.2. Szmajda V&V Signal Parameters

Input	Bandwidth (Hz)	Samp Freq f_s (Hz)	Duration (Sec)	Number of Samples	Sample Rate	Zero Padding
Original	4.00×10^4	1.00×10^2	5.00×10^1	5000	1	N/A
Resampled	4.00×10^4	3.00×10^5	1.12×10^2	15000000	3000	2^{25}

After pre-processing the Szmajda signal according to parameters in Table 4.2, the signal was input to the QMFB process. Representative QMFB results for Layer #18 are presented in Figure 4.4 which shows the discrete frequency responses in the signal. It can be seen that the signal started at $f = 5.0$ KHz and increased its power in the interval $13.0 < t < 25.0$ s. For the interval $25.0 < t < 37.0$ s there is no signal present, followed by

the interval $37.0 < t < 50.0$ s from 37 s to 50 s when three frequencies are present ($f = 5.0$ KHz, $f = 10.0$ KHz, and $f = 40.0$ KHz). The estimated frequency and time resolution parameters were computed from the F-T plot in Figure 4.4 as $\Delta f \approx 0.57$ KHz and $\Delta t \approx 0.88$ s. For the average frequency and time plots, the parameters are $\Delta f \approx 0.57$ KHz and $\Delta t \approx 13.65$ *m*s, respectively. By comparing analytic signal responses in Figure 4.3, both the average frequency and time responses from the QMFB process, with some degradation and loses due to the computing processing, was consistent.

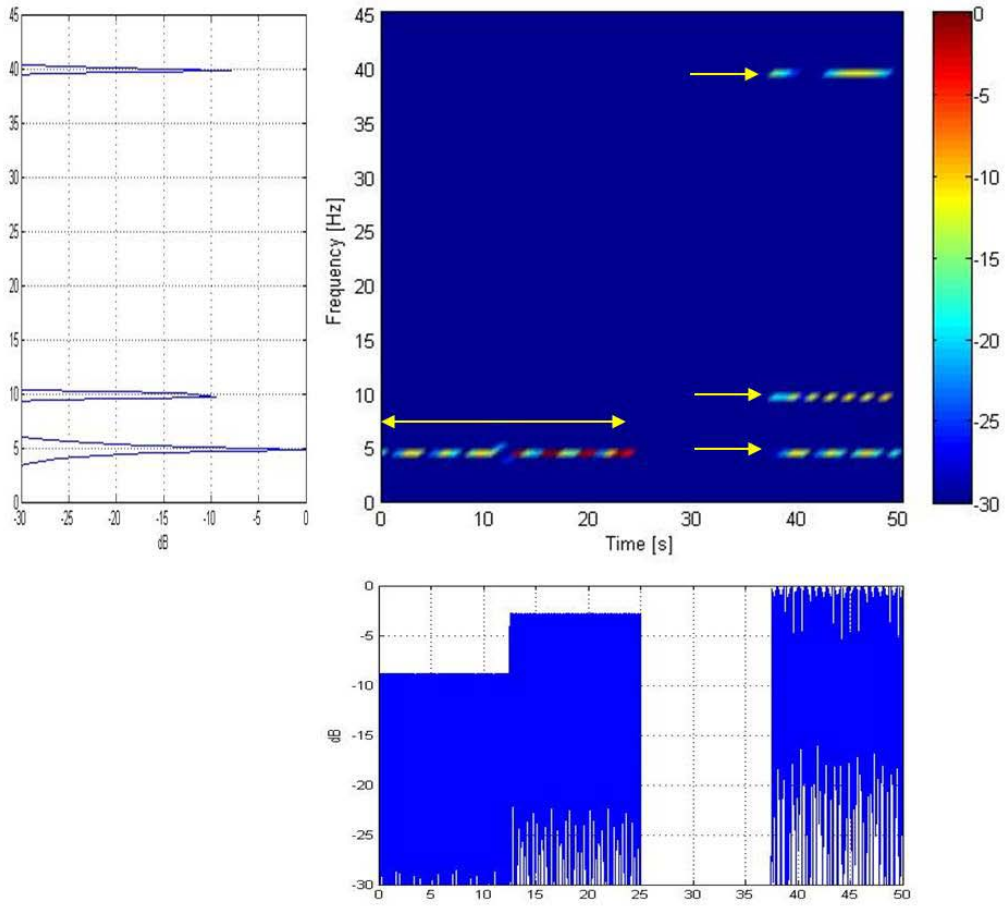

Figure 4.4. QMFB Layer #18 output for Szmajda V&V signal. Average PSD plot based on Layer #18 as presented and average time plot based on Layer #12.

After processing and analyzing QMFB performance using the V&V signals, it was concluded that the QMFB process is able to effectively process different types of signals and produce outputs matching theoretical expected results. However, some pre-QMFB filtering artifacts appeared due to the effects of instantaneous frequency on filter performance. Beside the artifacts, the QMFB results presented an acceptable response in frequency and time allocation within the middle layers.

4.3 OFDM-Based Signal Performance

The two OFDM-based signals described in Chapter 2 were used as input to the QMFB process and simulation performed according to the methodology explained in Chapter 3. Results for 802.11a Wi-Fi and 802.16e WiMAX OFDM-based signals are presented and QMFB output reliability assessed relative to input signal features. Overlay plots are computed to compare input signal and QMFB output responses for single burst and integrated burst response cases.

4.3.1 Experimental 802.11a Wi-Fi Signal

Experimental 802.11a Wi-Fi signal assessment was performed using data collected in support of previous work detailed in [8]. Collections were made using AFIT's RFSICS with the Wi-Fi devices operating in an anechoic chamber environment. According to the structure of this signal described in Chapter 2, the 802.11a signal is composed of two distinct regions. The *preamble* region is used for network synchronization, timing, control, etc., and the *payload* region is used for transferring user data. Per IEEE standards for 802.11a implementation [9], the preamble is further divided into two distinct regions, with the first half containing 10 short OFDM symbols and the

second half containing 2 long OFDM symbols. The 10 short OFDM symbols region is selected here for demonstration with a single burst sent to the QMFB process first and then an integrated collection of bursts sent to the QMFB process.

4.3.1.1 802.11a Wi-Fi Preamble

The normalized time and PSD responses for 802.11a Wi-Fi preamble are shown in Figure 4.5. The first ten symbols of the preamble were isolated, resampled and zero-padded prior to QMFB processing according to the values shown in Table 4.3. Related to the time response, the signal duration is approximate $T = 8$ μs and it can be seen that 10 peaks are very noticeable. Considering the W_{-30dB} bandwidth, the PSD response shows twelve distinct frequency components that match the 802.11a signal structure described in Chapter 2.

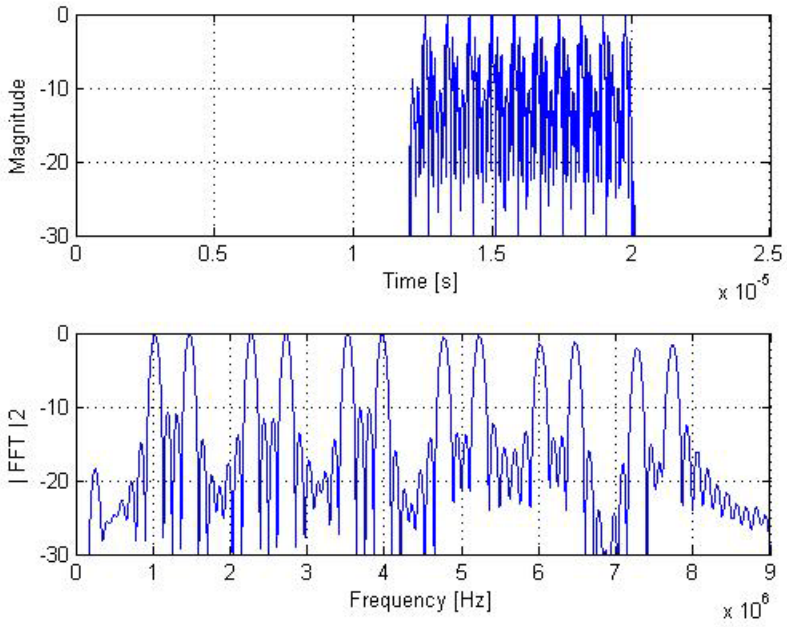

Figure 4.5 Time and PSD responses for 10 short symbols 802.11a Wi-Fi preamble.

Table 4.3. 802.11a 10 short symbols set as input to QMFB

Input	Bandwidth (Hz)	Samp Freq f_s (Hz)	Duration (Sec)	Number of Samples	Sample Rate	Zero Padding
Original	8.00×10^{6}	2.38×10^{7}	1.35×10^{-4}	3200	1	N/A
Resampled	8.00×10^{6}	2.38×10^{11}	1.41×10^{-4}	32000000	10000	2^{25}

The QMFB output for Layer #19 is shown in Figure 4.6. The allocations of twelve frequency components seen in Figure 4.5 are present. The estimated frequency and time resolution parameters were computed from the F-T plot in Figure 4.6 as $\Delta f \approx 113.25$ KHz and $\Delta t \approx 4.56$ µs. For the average frequency and time plots, the parameters are $\Delta f \approx 56.6$ KHz and $\Delta t \approx 0.069$ µs, respectively. Appendix C.1 presents a table of computed Δf and Δt resolutions as function of f_s for a given layer. It can be seen that the frequencies are allocated within the expected interval ($f = 1$ MHz to $f = 8$ MHz). The average time plot was computed using Layer #14 due to the F-T trade-off explained in Chapter 2 with better time resolution obtained in lower QMFB layers. The expected ten peaks are noticeable in the average time plot and are located approximately at the same expected times. However, the output signal magnitude response is between 1.0 and 2.0 dB lower when compared to the input signal in Figure 4.5.

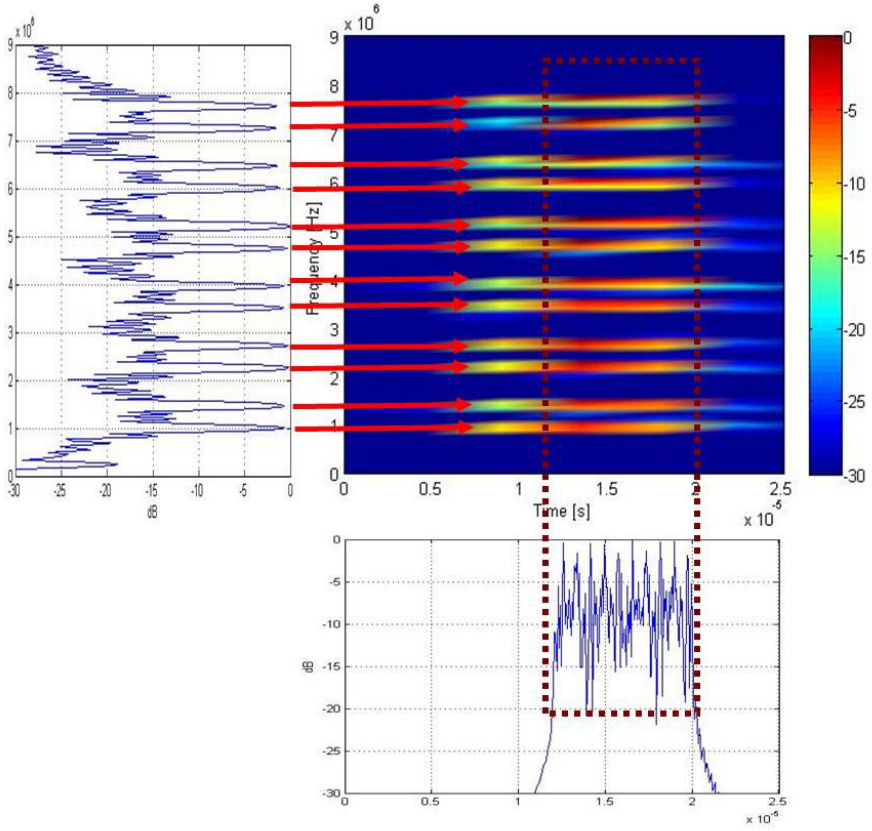

Figure 4.6 QMFB Layer #20 output for 10 short symbols of 802.11a Wi-Fi preamble. Average PSD based on Layer #21 as presented and average time based on Layer #14.

4.3.1.2 802.11a Wi-Fi Single Burst Response

The normalized time and PSD responses using a single 802.11a Wi-Fi burst are shown in Figure 4.7. The signal was resampled and zero-padded prior to QMFB processing according to the values shown in Table 4.4. Related to the time response, the signal duration is approximate $T = 11.6$ ms with ten visible peaks corresponding to the first half of the preamble. It can be seen that the rest of the signal presents a noise like behavior. The PSD response shows that the signal's frequency components, considering the $W_{-30\text{dB}}$ baseband bandwidth, the dominant frequency responses are located from $f = 0$

to f = 10 MHz. These initial results matched the signal structure described in Chapter 2.

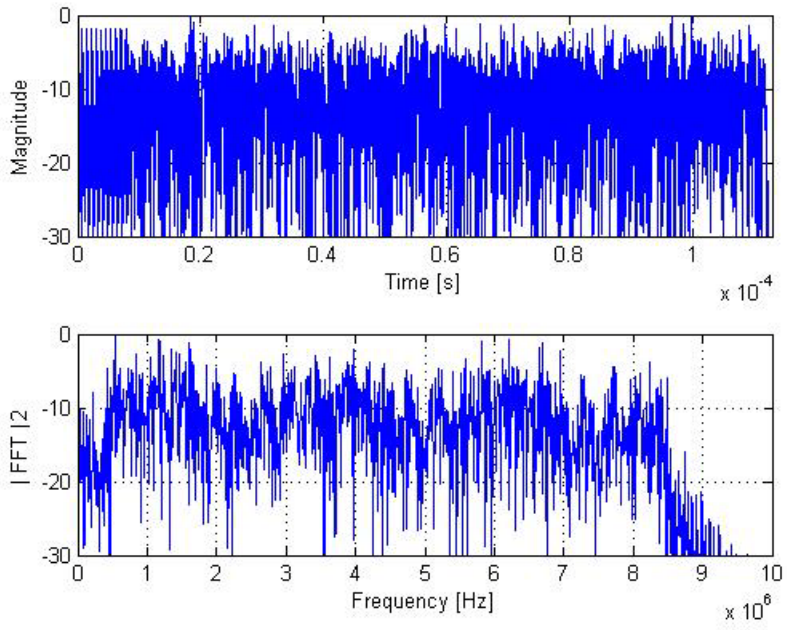

Figure 4.7 Time and PSD responses for single 802.11a Wi-Fi burst.

Table 4.4. 802.11a single burst signal values set as input to QMFB

Input	Bandwidth (Hz)	Samp Freq f_s (Hz)	Duration (Sec)	Number of Samples	Sample Rate	Zero Padding
Original	$9.00\text{x}10^{6}$	$2.38\text{x}10^{7}$	$1.24\text{x}10^{-4}$	2945	1	N/A
Resampled	$9.00\text{x}10^{6}$	$2.38\text{x}10^{10}$	$1.77\text{x}10^{-4}$	2945000	1000	2^{22}

The QMFB output for Layer #16 is shown in Figure 4.8. The allocations of multiple frequency components seen in Figure 4.7 are present. The estimated frequency and time resolution parameters were computed from the F-T plot in Figure 4.8 as $\Delta f \approx 181.12$ KHz and $\Delta t \approx 2.8$ μs. For the average frequency and time plots, the parameters are $\Delta f \approx 11.3$ KHz and $\Delta t \approx 21.56$ *n*s, respectively. Appendix C.2 presents a table of computed Δf and Δt resolutions as function of f_s for a given layer. It can be seen that frequencies are allocated within the expected interval (f = 1 MHz to f = 10 MHz).

The first half of the preamble response is still noticeable and is located approximately at the same expected times compared to the input shown in Figure 4.7.

According to the 802.11a signal parameters described in Chapter 2, there are some signal features that can be extracted through qualitative visual assessment of the QMFB output shown in Figure 4.8:

- The 10 short symbols shown in the left-hand red dashed rectangle
- The guard Interval shown in the right-hand red dashed rectangle

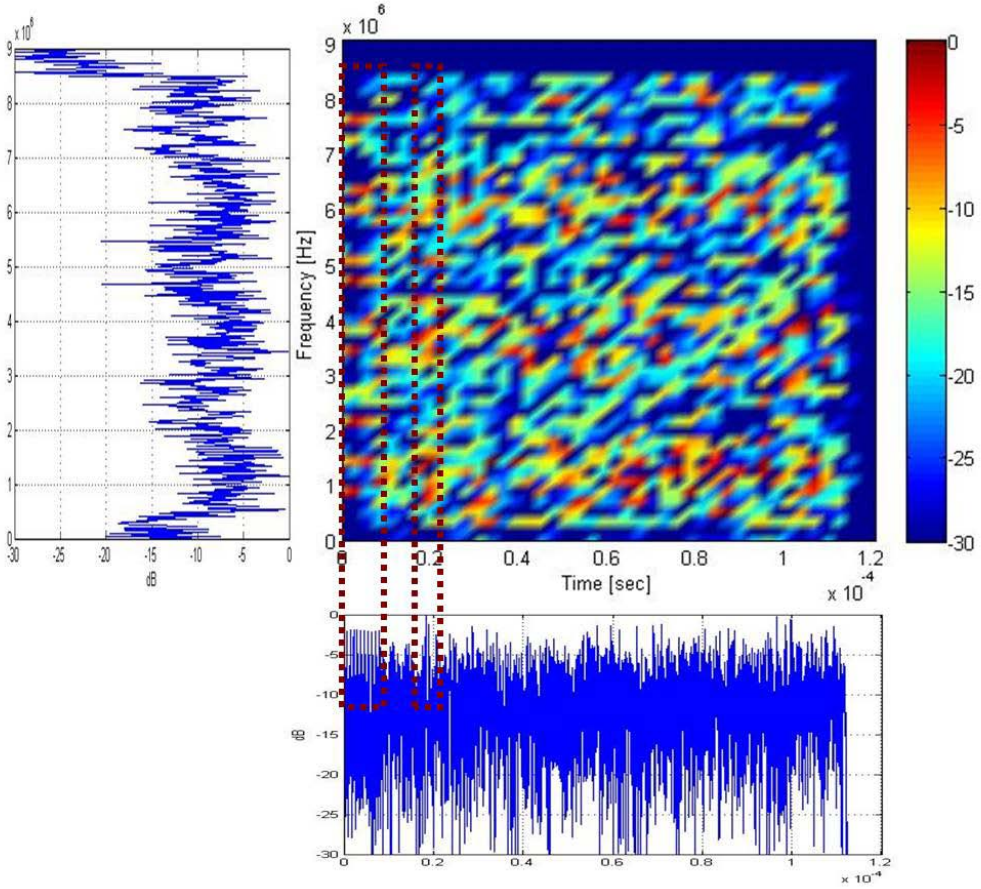

Figure 4.8 QMFB Layer #16 output for *single* 802.11a Wi-Fi burst. Average PSD based on Layer #20 as presented and average time based on Layer #9.

4.3.1.3 Wi-Fi Integrated Burst Response

The normalized time and PSD responses for integrated 802.11a bursts are shown in Figure 4.9. In this case, a total of $N_B = 500$ 802.11a burst responses were integrated to create a new input to the QMFB process. The signal was resampled and zero-padded prior to QMFB processing according to the values shown in Table 4.5. Related to the time response, the signal duration is approximate $T = 11.6$ ms with ten visible peaks corresponding to the first half of the preamble and the rest of the signal presents a noise like behavior. The PSD response shows that the signal's frequency components, considering the $W_{-30\text{dB}}$ baseband bandwidth, the dominant frequency responses are located from $f = 0$ to $f = 10$ MHz. These results match the signal structure described in Chapter 2. It also can be seen that the first ten symbols show a uniform magnitude, with the peak located at approximately at $t = 2.4$ μs corresponding to the guard interval described in Chapter 2. The part of the signal corresponding to the payload (user data) shows a magnitude reduction due to randomness of the symbol assignment.

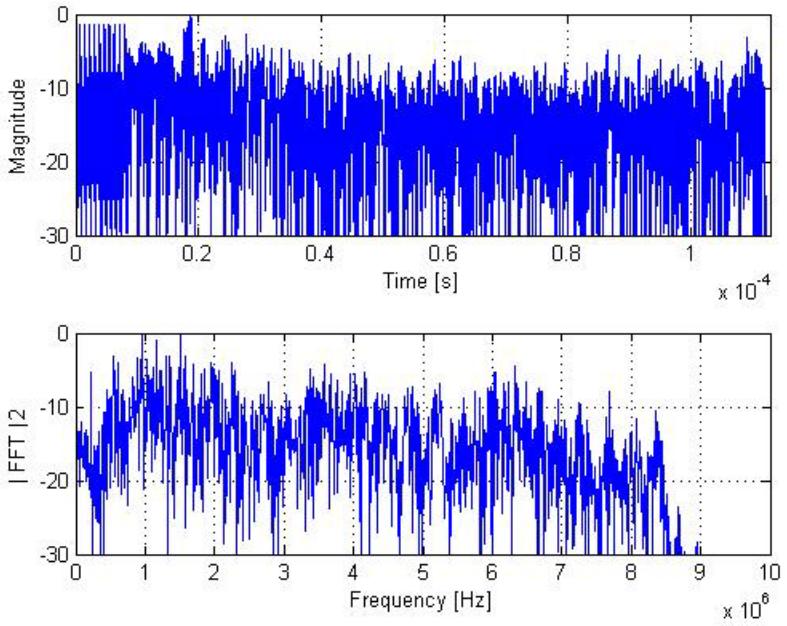

Figure 4.9 Time and PSD responses for N_B = 500 integrated bursts 802.11a Wi-Fi.

Table 4.5. 802.11a signal values for N_B = 500 integrated bursts as input to QMFB

Input	Bandwidth (Hz)	Samp Freq f_s (Hz)	Duration (Sec)	Number of Samples	Sample Rate	Zero Padding
Original	$9.00\text{x}10^{6}$	$2.38\text{x}10^{7}$	$1.24\text{x}10^{-4}$	2945	1	N/A
Resampled	$9.00\text{x}10^{6}$	$2.38\text{x}10^{10}$	$1.77\text{x}10^{-4}$	2945000	1000	2^{22}

The QMFB output for Layer #16 is shown in Figure 4.10for integration of N_B = 500 bursts. The allocation of multiple frequencies components seen in Figure 4.9 is present. The estimated frequency and time resolution parameters were computed from the F-T plot in Figure 4.10 as $\Delta f \approx 181.12$ KHz and $\Delta t \approx 2.8$ µs. For the average frequency and time plots, the parameters are $\Delta f \approx 22.6$ KHz and $\Delta t \approx 0.173$ µs, respectively. Appendix C.2 presents a table of computed Δf and Δt resolutions as function of f_s for a given layer. The first half of the preamble response is still noticeable and is located approximately at the same expected times compared to the input shown in Figure 4.9.

According to the 802.11a signal parameters described in Chapter 2, there are some signal features that can be extracted through qualitative visual assessment of the QMFB output shown in Figure 4.10:

- The 10 short symbols shown in the left-hand red dashed rectangle
- Lower correlation in the payload (user data) region in the right-hand red dashed rectangle
- Average signal power below -5.0 dB for the payload (user data) region highlighted by a red arrow in the average time plot.

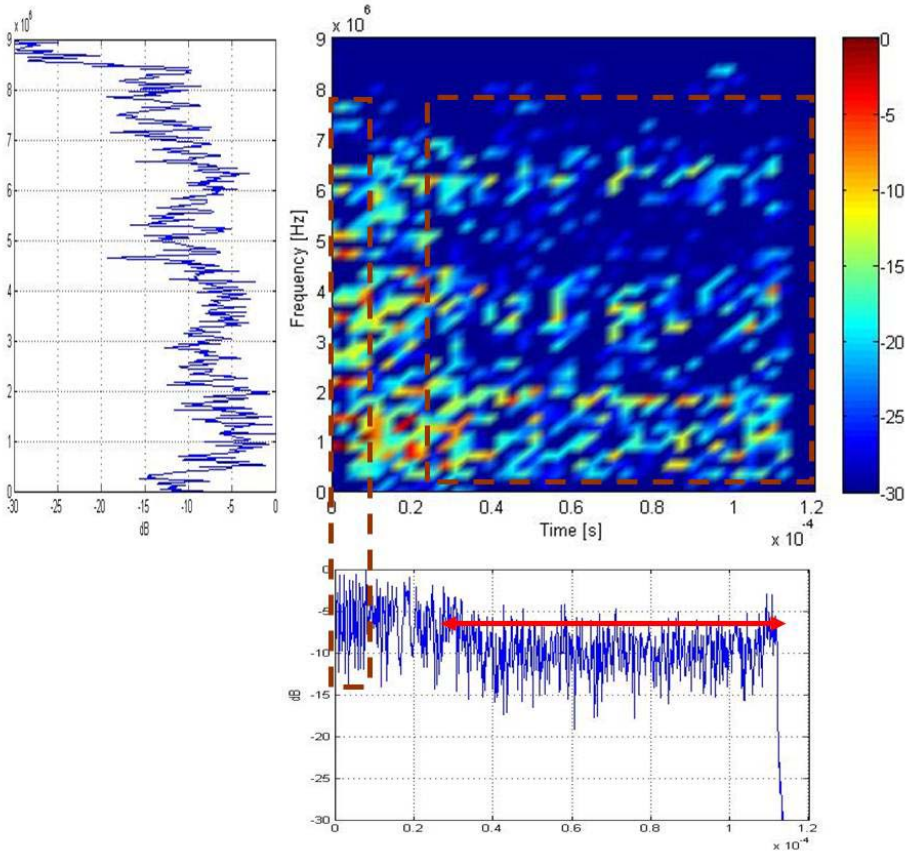

Figure 4.10 QMFB Layer #16 output for N_B = 500 *integrated* Wi-Fi bursts. Average PSD plot based on Layer #19 as presented and average time plot based on Layer #12.

4.3.1.4 802.11a Wi-Fi Preamble: Single vs. Integrated Response

To assess the QMFB response relative to signal input features, average time and frequency plots are provided in Figure 4.11 to Figure 4.14 for single burst and integrated burst QMFP processing. Related to the overlaid time responses in Figure 4.11 and Figure 4.12, it can be seen that the QMFB output envelope matches the input time response for both single and integrated burst cases. Therefore, the F-T plots computed during the process are reliable for revealing 802.11a Wi-Fi signal characteristics. In the payload (user data) region of the average time response ($t > 200$ μs), the power reduction for burst integration is evident given the random signal structure in this region. Related to the average PSD response presented in Figure 4.13 and Figure 4.14, the burst integration resulted in gain of approximate $G \approx 3.0$ dB when compared to the input signal or single burst QMFB responses.

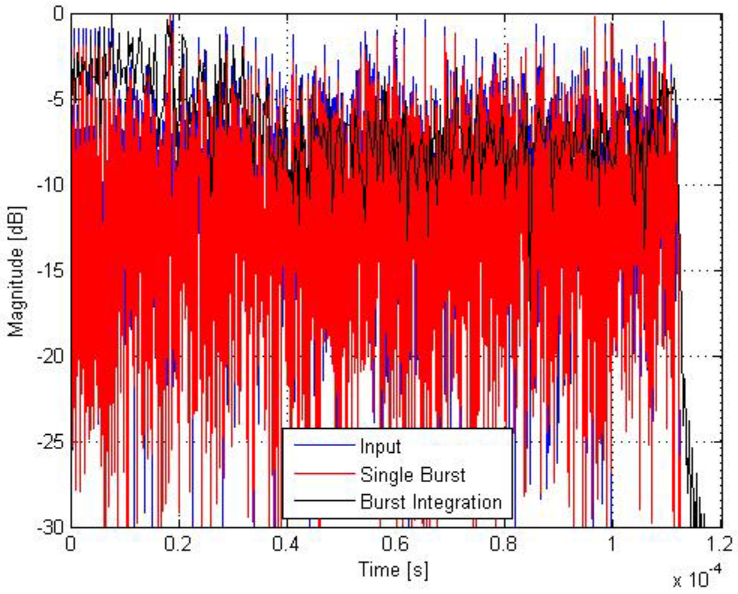

Figure 4.11 Average time responses for 802.11a Wi-Fi signal.

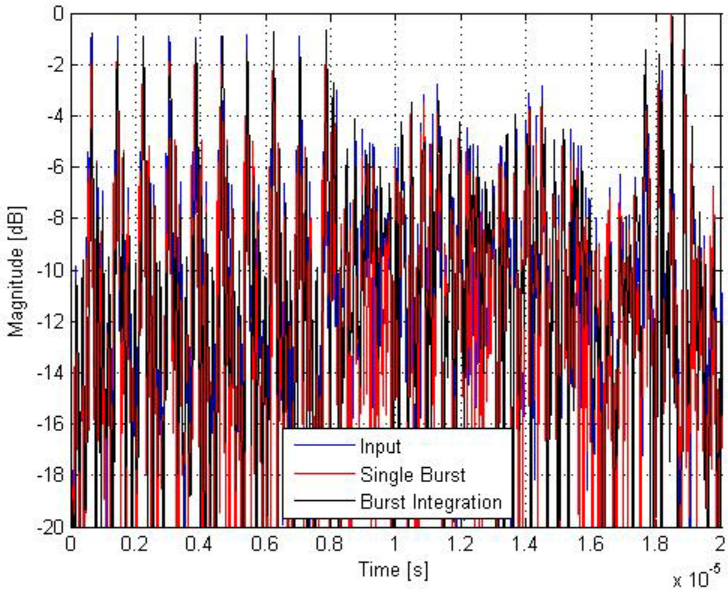

Figure 4.12 Average time responses for 802.11a Wi-Fi signal expanded region for $0 < t < 200$ μs.

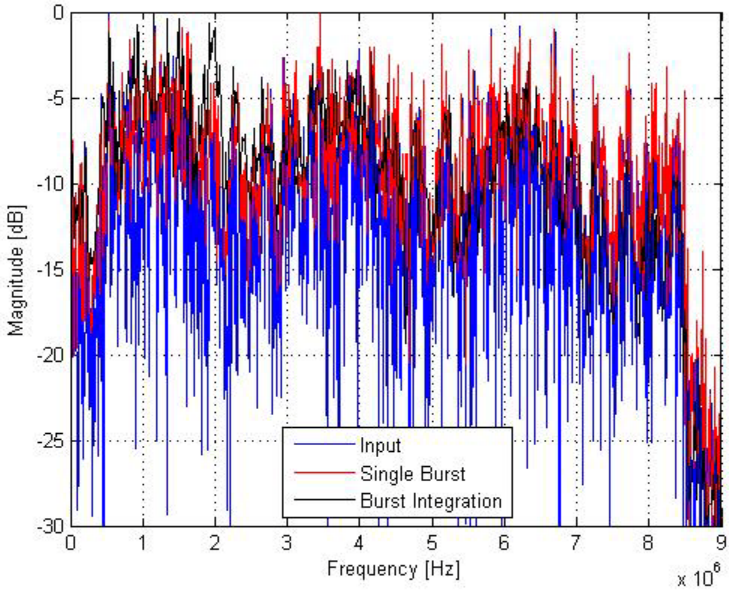

Figure 4.13 Average PSD responses for 802.11a Wi-Fi signal.

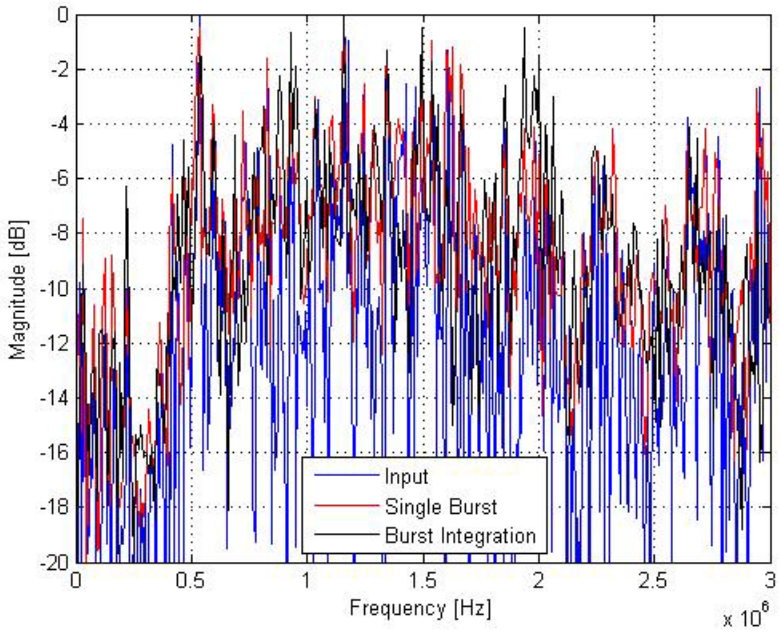

Figure 4.14 Average PSD responses for 802.11a Wi-Fi signal expanded region for $0 < f < 3$ MHz.

4.3.2 Experimental 802.16e WiMAX Signal

Experimental 802.16e WiMAX signal assessment was performed using data collected in support of previous work detailed in [0, 11]. The collections were obtained using AFIT's RFSICS with Alvarion BreezeMAX 5000 Mobile Subscriber (MS) devices operating in a typical office environment [13]. According to the structure of this signal described in Chapter 2, and experimental observations noted in [0, 11], the analysis was divided in two parts. The first part only considers WiMAX *range-only* burst responses and the second part considers only WiMAX *data-only* burst responses. For each of these cases, QMFB processing is conducted using single burst and integrated burst responses.

4.3.2.1 WiMAX *Range-Only* Burst: Single Response

The normalized time and PSD responses using a single *range-only* WiMAX burst are shown in Figure 4.15. The signal was resampled and zero-padded prior to QMFB processing according to the values shown in Table 4.6. Related to the time response, the signal duration is approximately $T = 0.4$ *m*s and, considering the W_{-30dB} bandwidth, the PSD response clearly shows some frequency components located in three spectral regions, including: $0 < f < 0.4$ MHz, $0.6 < f < 1.0$ MHz and $1.6 < f < 2.0$ MHz.

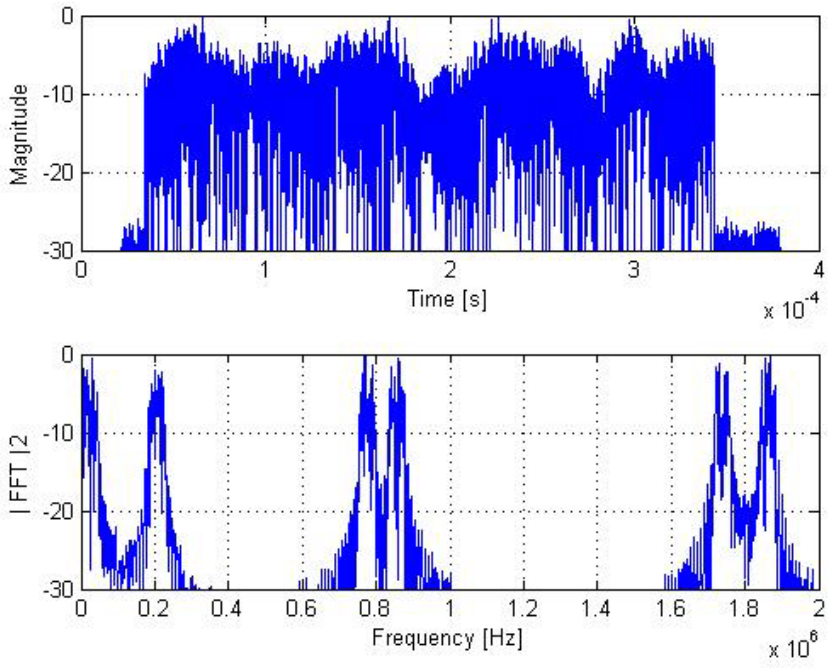

Figure 4.15. Time and PSD responses for *single* 802.16e WiMAX *range-only* burst.

Table 4.6. 802.16e WiMAX range-only single burst parameters

Input	Bandwidth (Hz)	Samp Freq f_s (Hz)	Duration (Sec)	Number of Samples	Sample Rate	Zero Padding
Original	2.00×10^6	1.19×10^7	3.81×10^{-4}	4521	1	N/A
Resampled	2.00×10^6	3.56×10^{10}	9.42×10^{-4}	13563000	3000	2^{25}

The QMFB output for Layer #18 is shown in Figure 4.16 for single 802.16e WiMAX *range-only* burst. The allocation of six frequencies components seen in Figure 4.15 is present. The estimated frequency and time resolution parameters were computed from the F-T plot in Figure 4.16 as $\Delta f \approx 67.9$ KHz and $\Delta t \approx 7.4$ μs. For the average frequency and time plots, the parameters are $\Delta f \approx 16.9$ KHz and $\Delta t \approx 0.115$ μs, respectively. Appendix C.3 presents a table of computed Δf and Δt resolutions as function of f_s for a given layer. It can be seen that frequencies are allocated within the three expected intervals ($0 < f < 0.4$, $0.6 < f < 1.0$, and $1.6 < f < 2.0$ MHz), are distributed in three pairs, and span the bandwidth shown in Figure 4.15. Within each pair of frequencies a transition is seen between a certain numbers of transmitted symbols.

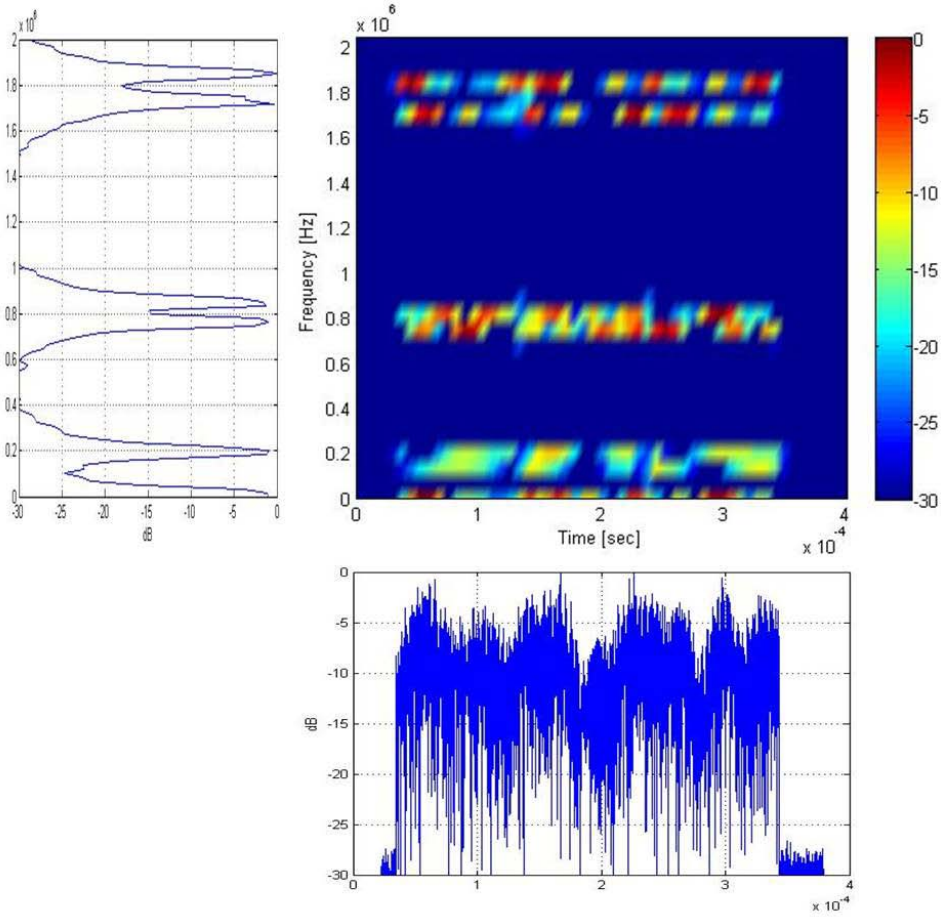

Figure 4.16 QMFB Layer #18 output for *single* 802.16e WiMAX *range-only* burst. Average PSD plot based on Layer #20 and average time plot based on Layer #12.

4.3.2.2 WiMAX *Range-Only* Burst: Integrated Response

The normalized time and PSD responses using integrated *range-only* WiMAX bursts are shown in Figure 4.17. In this case, a total of $N_B = 1400$ 802.16e burst responses were integrated to create a new input to the QMFB process. The range-only integrated burst signal was resampled and zero-padded prior to QMFB processing according to the same values previously shown in Table 4.6. Related to the time response, the signal duration is approximately $T = 0.4$ ms and, considering the $W_{-30\text{dB}}$

bandwidth, the PSD response contains the same frequency components as the single burst response ($0 < f < 0.4$ MHz, $0.6 < f < 1.0$ MHz and $1.6 < f < 2.0$ MHz) plus some additional frequency components below the P = -20 dB level.

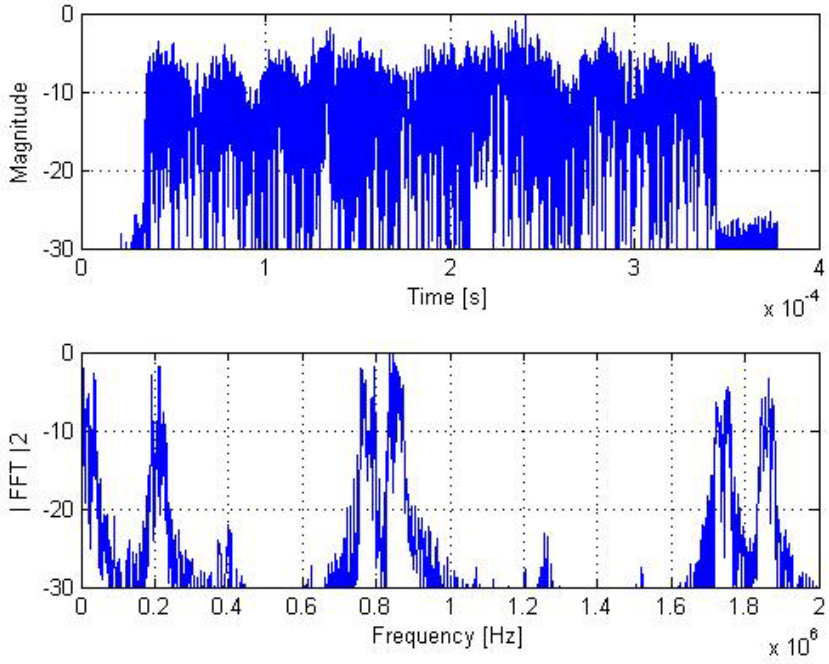

Figure 4.17. Time and PSD responses for N_B = 1400 *integrated* 802.16e WiMAX *range-only* bursts.

The QMFB output for Layer #18 is shown in Figure 4.18 for $N_B = 1400$ integrated 802.16e WiMAX *range-only* bursts. The allocation of six frequencies components seen in Figure 4.17 is present. The estimated frequency and time resolution parameters were computed from the F-T plot in Figure 4.18 as $\Delta f \approx 67.9$ KHz and $\Delta t \approx 7.4$ μs. For the average frequency and time plots, the parameters are $\Delta f \approx 16.9$ KHz and $\Delta t \approx 0.115$ μs, respectively. Appendix C.3 presents a table of computed Δf and Δt resolutions as function of f_s for a given layer. It can be seen that frequencies are allocated within the three expected intervals ($0 < f < 0.4$, $0.6 < f < 1.0$, and $1.6 < f < 2.0$ MHz), are

distributed in three pairs, and span the bandwidth shown in Figure 4.17. In this case, the middle pair of frequencies presented the higher power correlation compared to the other frequency components.

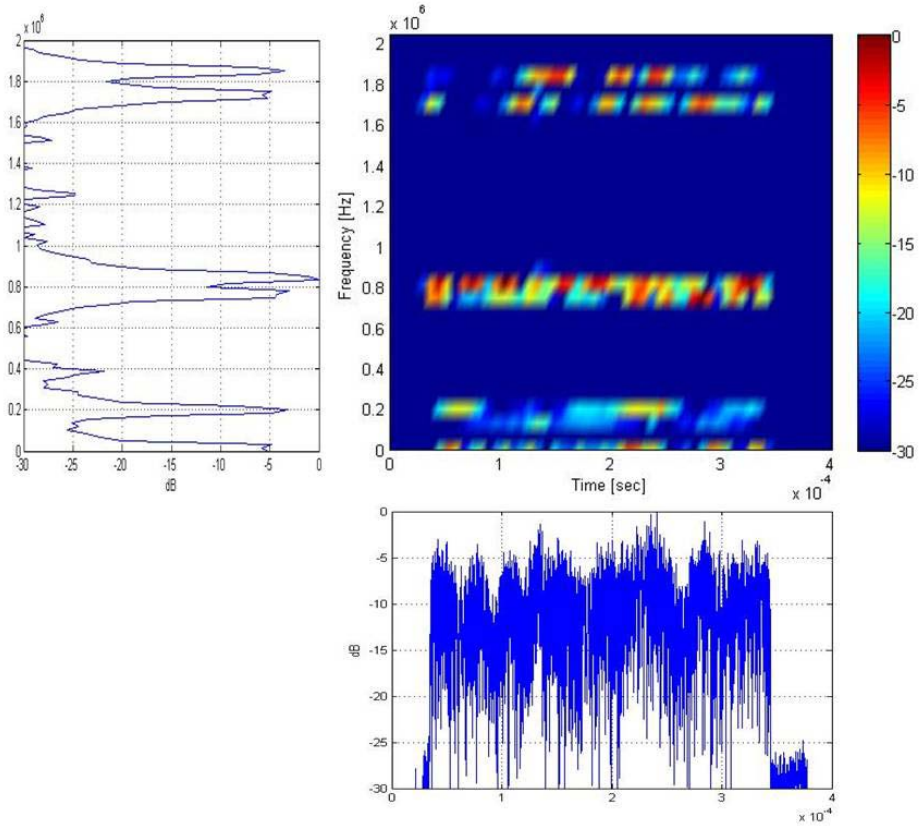

Figure 4.18 QMFB Layer #18 output for N_B = 1400 *integrated* 802.16e WiMAX *range-only* bursts. Average PSD based on Layer #20 and average time based on Layer #12.

4.3.2.3 WiMAX *Range-Only* Burst: Single vs. Integrated Response

To assess the QMFB response relative to input signal features, average time and frequency plots are provided in Figure 4.19 to Figure 4.22 for single burst and integrated burst QMFP processing. Related to the overlay time response in Figure 4.19 and Figure 4.20, the integrated burst QMFB output show less energy in the time response due to

integration of random symbol assignment within and across every integrated burst. Related to overlay PSD responses in Figure 4.21 and Figure 4.22, it can be seen that the W_{-30dB} bandwidth remains constant and that burst integration resulted in "thinner" responses for the six frequency components.

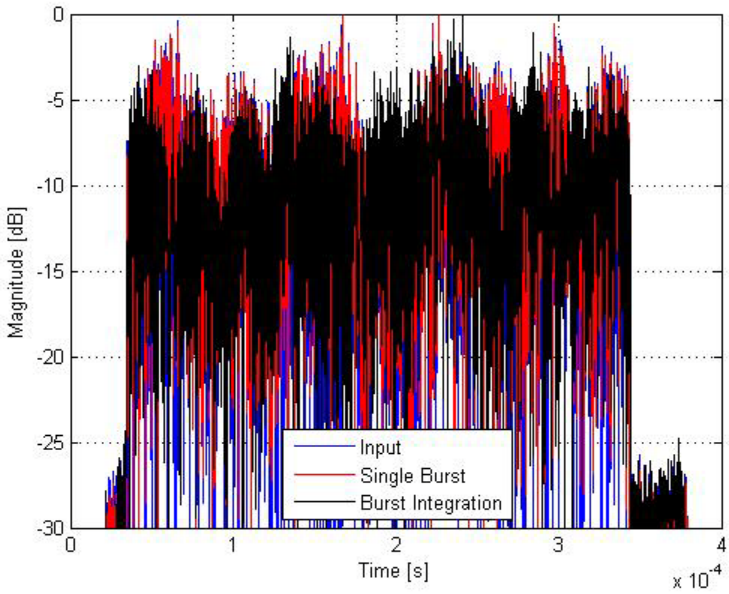

Figure 4.19 Average time responses for 802.16e WiMAX *range-only* burst.

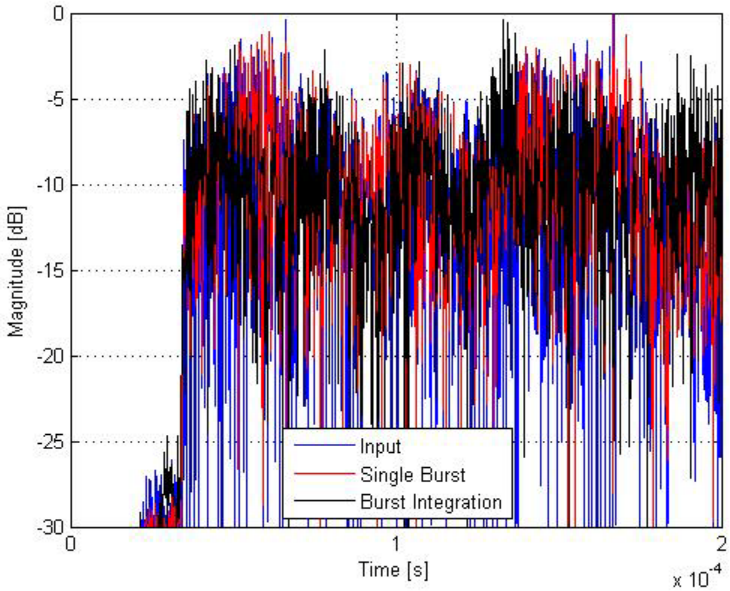

Figure 4.20 Average time responses for 802.16e WiMAX *range-only* burst. Expanded region for $0 < t < 200$ μs.

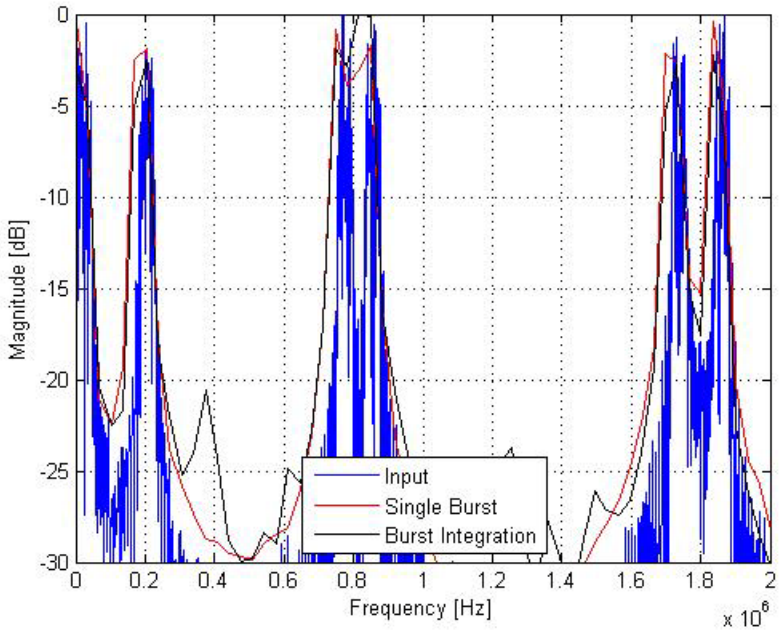

Figure 4.21 Average PSD responses for 802.16e WiMAX *range-only* burst.

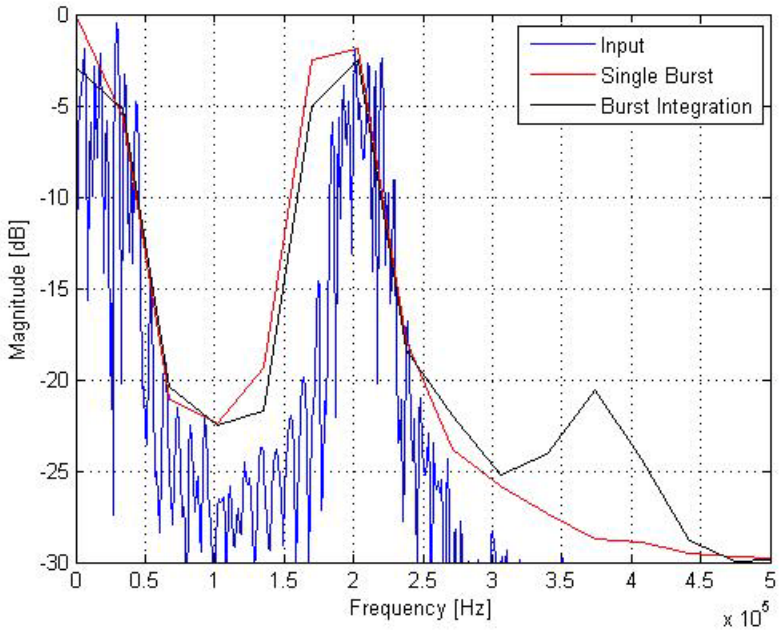

Figure 4.22 Average PSD responses for 802.16e WiMAX *range-only* burst. Expanded region for $0 < f < 0.5$ MHz.

4.3.2.4 802.16e WiMAX *Data-Only* Burst: Single Response

The normalized time and PSD responses using a single *data-only* 802.16e WiMAX burst is shown in Figure 4.23. The signal was resampled and zero-padded prior to QMFB processing according to the values shown in Table 4.7. Related to the time response, the signal duration is approximate $T = 1.6$ ms and the noise like behavior of the signal is seen in both time and frequency responses.

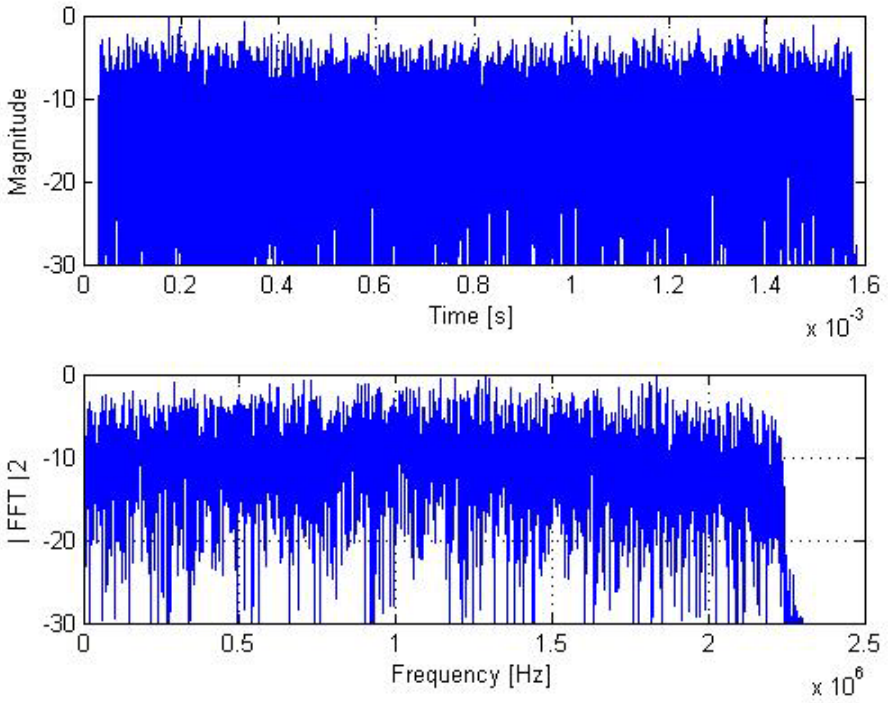

Figure 4.23 Time and PSD responses for *single* 802.16e WiMAX *data-only* burst.

Table 4.7. 802. 16e WiMAX data-only single burst parameters

Input	Bandwidth (Hz)	Samp Freq f_s (Hz)	Duration (Sec)	Number of Samples	Sample Rate	Zero Padding
Original	$2.50\text{x}10^{6}$	$1.19\text{x}10^{7}$	$1.61\text{x}10^{-3}$	19125	1	N/A
Resampled	$2.50\text{x}10^{6}$	$1.19\text{x}10^{10}$	$2.83\text{x}10^{-3}$	19125000	1000	2^{25}

The QMFB output for Layer #16 is shown in Figure 4.24 for a single 802.16e WiMAX *range-only* burst. The multiple frequency allocations shown in Figure 4.23 are present. The estimated frequency and time resolution parameters were computed from the F-T plot in Figure 4.24 as $\Delta f \approx 90.6$ KHz and $\Delta t \approx 5.53$ µs. For the average frequency and time plots, the parameters are $\Delta f \approx 5.66$ KHz and $\Delta t \approx 0.345$ µs, respectively. Appendix C.3 presents a table of computed Δf and Δt resolutions as function

of f_s for a given layer. Other than bandwidth ($W_{\text{-30dB}} \approx 2.25$ MHz) and signal duration ($T \approx 1.6$ ms), no signal structure can be extracted from the F-T plot.

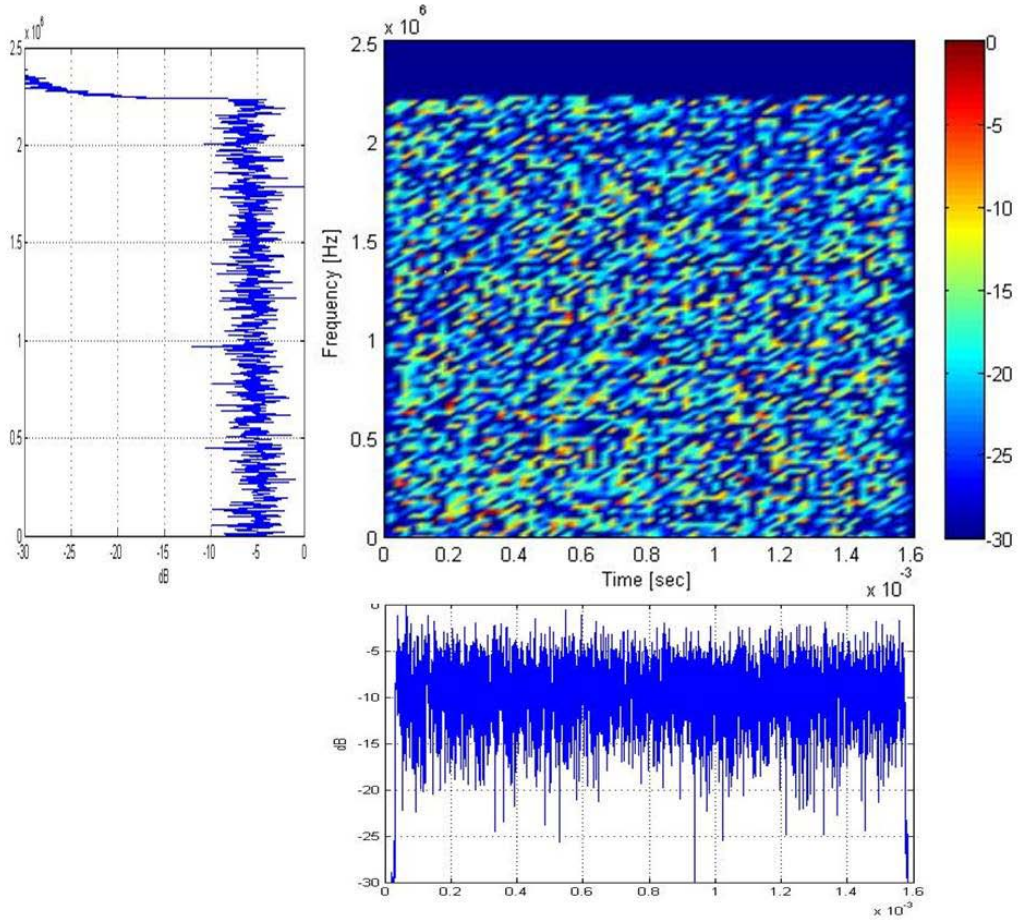

Figure 4.24 QMFB Layer #16 output for *single* 802.16e WiMAX *data-only* burst. Average PSD based on Layer #20 and average time based on Layer #12.

4.3.2.5 802.16e WiMAX *Data-Only* Burst: Integrated Response

The normalized time and PSD responses for integrated *data-only* WiMAX bursts are shown in Figure 4.25. The signal was resampled and zero-padded prior to QMFB processing according to the values previously shown in Table 4.7. Related to the time response, the signal duration is approximate 1.6 ms and it can be seen the noise like behavior of the signal in both time and frequency responses.

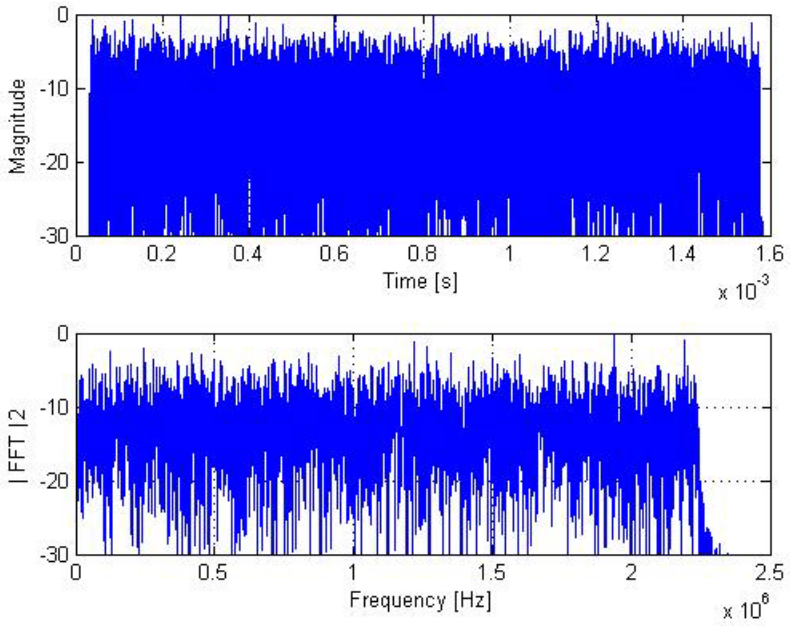

Figure 4.25 Time and PSD responses for N_B = 640 *integrated* 802.16e WiMAX *data-only* bursts.

The QMFB output for Layer #16 is shown in Figure 4.26 for N_B = 640 integrated 802.16e WiMAX *data-only* bursts. The allocation of multiple frequencies components seen in Figure 4.25 is present. The estimated frequency and time resolution parameters were computed from the F-T plot in Figure 4.26 as $\Delta f \approx 90.6$ KHz and $\Delta t \approx 5.53$ µs. For the average frequency and time plots, the parameters are $\Delta f \approx 5.66$ KHz and $\Delta t \approx 0.345$ µs, respectively. Appendix C.3 presents a table of computed Δf and Δt resolutions as function of f_s for a given layer. Other than bandwidth ($W_{-30dB} \approx 2.25$ MHz) and signal duration ($T \approx 1.6$ ms), no signal structure can be extracted from the F-T plot.

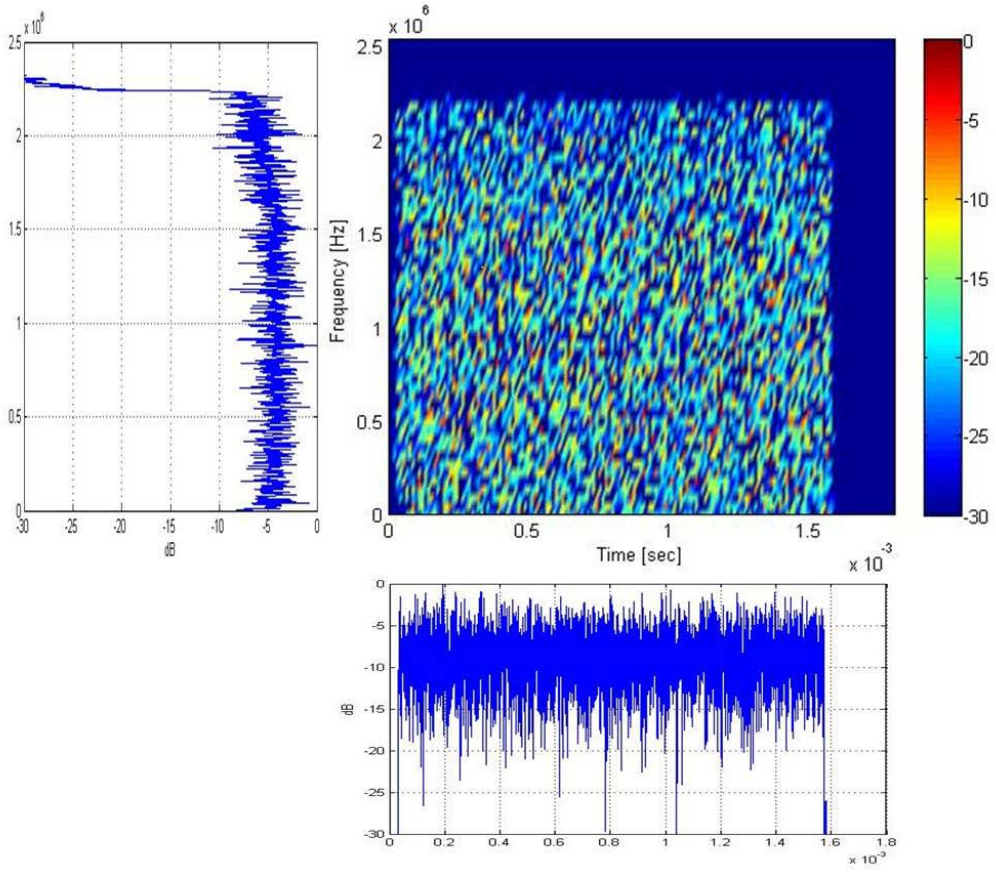

Figure 4.26 QMFB Layer #16 output for N_B = 640 *integrated* 802.16e WiMAX *data-only* bursts. Average PSD based on Layer #20 and average time based on Layer #12.

4.3.2.6 802.16e WiMAX *Range-Only* Burst: Single vs. Integrated Response

To assess the QMFB response relative to input signal features, average time and frequency plots are provided in Figure 4.27 to Figure 4.30 for single burst and integrated burst QMFP processing. Related to the overlaid time responses in Figure 4.27 and Figure 4.28 the integrated burst QMFB output shows less energy in the time response due to integration of random symbol assignment within and across every integrated burst. Related to the PSD responses in Figure 4.29 and Figure 4.30, it can be seen that the bandwidth is constant along the burst integration.

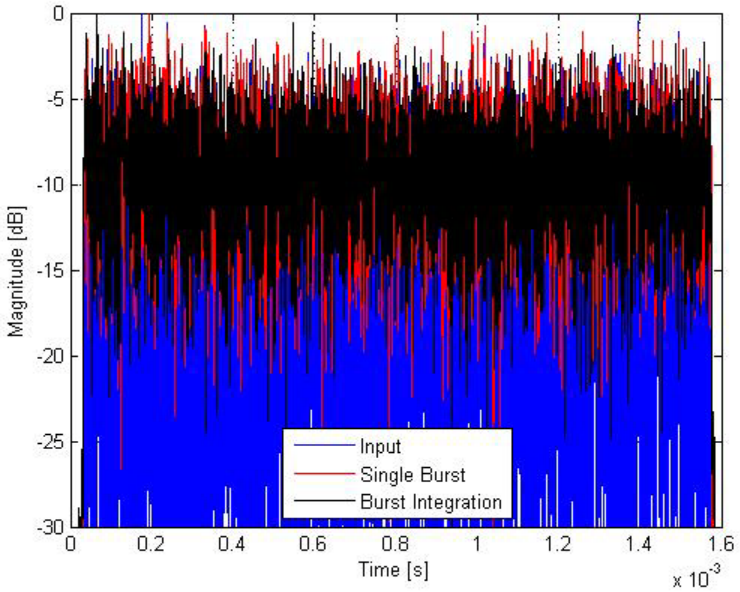

Figure 4.27 Average time responses for 802.16e WiMAX *data-only* burst

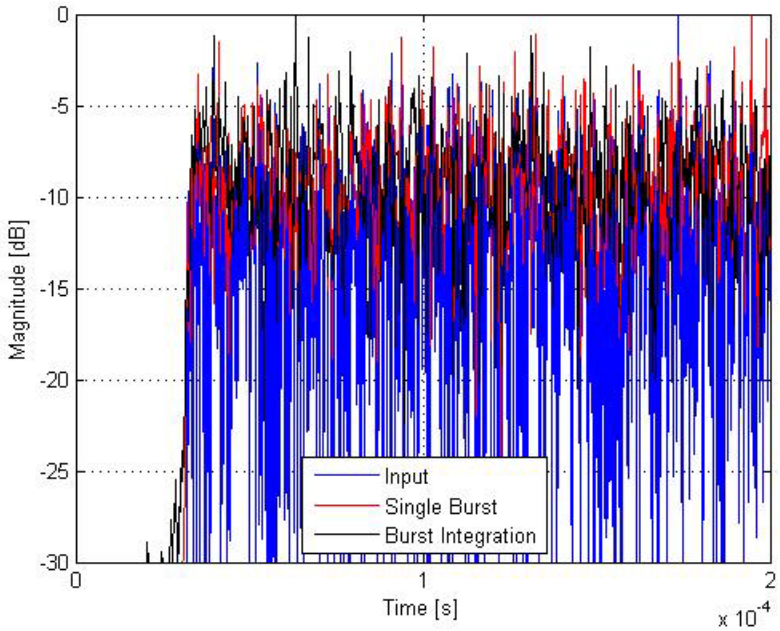

Figure 4.28 Average time responses for 802.16e WiMAX *data-only* burst. Expanded region for $0 < t < 200$ μs (Bottom).

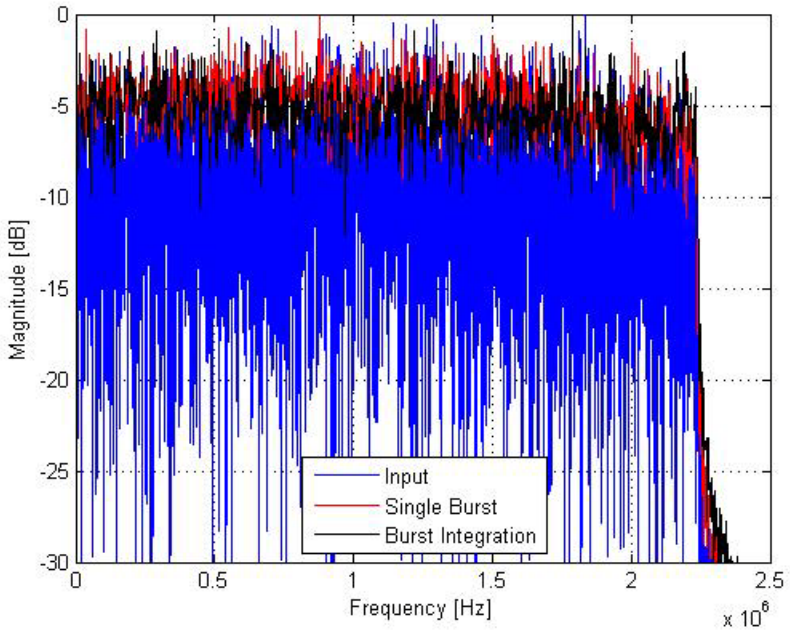

Figure 4.29 Average PSD responses for 802.16e WiMAX *data-only* burst.

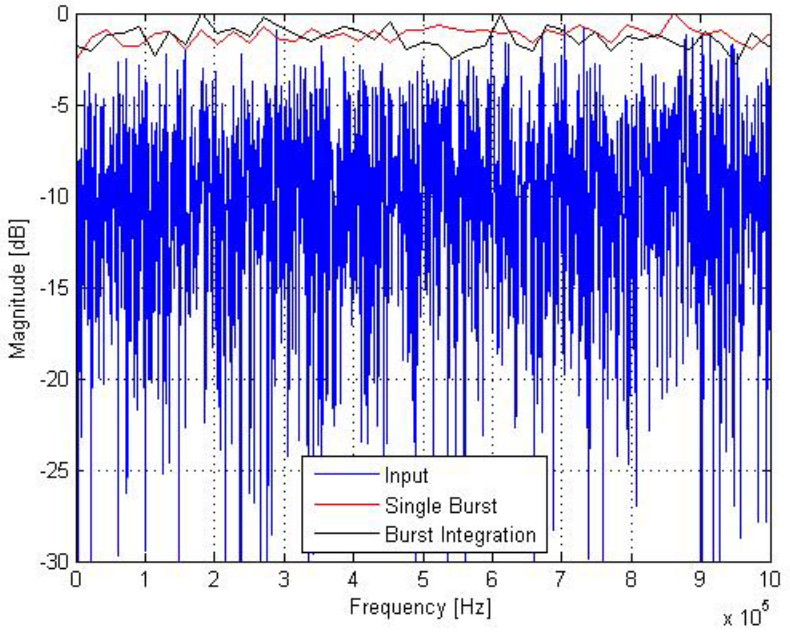

Figure 4.30 Average PSD responses for 802.16e WiMAX *data-only* burst. Expanded region for $0 < f < 1.0$ MHz.

4.4 Summary

The results presented in this chapter enabled qualitative visual assessment of QMFB performance using each signal of interest. Related to the LFM and Szmajda V&V signals, it was seen that the QMFB output offers reliable estimation of frequency and time characteristics. Once the baseline was defined, verified and validated, experimental OFDM-based signals were introduced and QMFB performance assessed. MATLAB® simulation results and qualitative visual analysis were sufficient for identifying some signal features such as signal duration (T_S) and bandwidth (W_{-30dB}) while highlighting relative signal structure.

Related to the analyzed 802.11a Wi-Fi signal, the preamble structure revealed by QMFB processing is consistent with the theoretical description in Chapter 2. Using burst integration, the effect of random symbol assignment during the payload (user data) region became evident as lower magnitude responses in Figure 4.10. The average time and average frequency plot showed that the QMFB output envelope followed the original signal behavior, but average loses of approximate 1.0 dB for burst integration and 2.0 dB for single burst were observed.

Related to the analyzed 802.16e WiMAX signal, the results are consistent with the framework defined in Chapter 2 and the QMFB output for both the ranging-on and data-only cases enabled qualitative visual assessment and provided some exploitation benefit. Some key signal features such as bandwidth, frequency and time allocation were extractable, and after further layer analysis approximations to symbol duration and channel bandwidth were available.

CHAPTER 5.

Summary, Conclusions and Recommendations

This chapter presents a summary and conclusions of research findings along with some recommendations for future work that have been extracted as result of this research effort. The chapter is divided in three subsections: 1) Section 5.1 presents a summary review related to the topics of interest covered during the research with some key exploitation concepts highlighted relative to the overall process; 2) Section 5.2 presents conclusions extracted from results after applying the adopted methodology in Chapter 3 and the baseline definitions given in chapter 2; and, 3) Section 5.3 is aimed at identifying other applications for QMFB exploitation providing recommendations for future work.

5.1 Summary

Chapter 1 presented the operational and technical motivation along with the research objectives. Related to the operational motivation, the approach was to provide a qualitative visual assessment process for a given signal from an operator's perspective. By performing QMFB processing with a given signal it is possible to obtain frequency-time (F-T) plots [1, 3, 4] having features that represent signal features such as bandwidth (W), center frequency (f_c), signal duration (T_s), modulation type (AM, FM, BPSK, QAM, etc), frequency content and time allocation. Because of its unique structure, two widely used signals based on Orthogonal Frequency Division Multiplexing (OFDM) were chosen as signals of interest for demonstration. The operational motivation relies on optimizing the QMFB process for the two signals of interest having defined structure according to [9, 12].

Chapter 2 presented the necessary technical background aimed at describing the topics of interest related to the operational and technical motivation. The general implementation of the QMFB process was described and implementation parameters and assumptions were made. The basic structure of OFDM signals was introduced next related to the physical layer perspective of 802.011a Wi-Fi and 802.16e WiMAX frame structures.

Chapter 3 presented the adopted methodology aimed at satisfying the defined research objectives using the technical details described in Chapter 2. An overall process overview was presented and the Verification and Validation (V&V) signals were described [2, 7]. The 802.011a Wi-Fi and 802.16e WiMAX experimental signals parameters were addressed [8, 0, 11, 13] and the initial QMFB configuration was established. The effect of resampling and zero-padding was described and measurable outputs were defined. Finally, the graphical presentation format for QMFB results was introduced.

Chapter 4 presented computed simulation results that were obtained after applying the defined methodology to each signal of interest. Initial time domain and frequency domain responses were presented for each input signal along with the initial and computed resampled parameters for each case. Results for selected QMFB outputs were presented according to the process introduced in Chapter 3 using 2D T-F QMFB plots and 1D average frequency and average time plots. Overlay plots of the 1D responses were computed and the input signal and output QMFB responses compared using a single burst and multiple integrated bursts. Time window resolution (Δt) and frequency window

resolution (Δf) parameters were extracted from each computed QMFB layer output.

5.2 Conclusions

Computed QMFB outputs were generated for all interest signals according to the adopted methodology. The QMFB process was implemented and decomposed successfully according to the defined measurable outputs. The following conclusions are presented based on the defined measurable outputs presented in Chapter 3:

1. *Layer Generation Minimization*

   Because higher number QMFB layers did not improve qualitative analysis, or did not give any additional information due to coarser Δt resolution when compared with lower numbered layers, the last three QMFB layers were not computed. Related to complete layer processing, this reduced overall computation time by approximate 78% when $N_Q = 22$ total layers were available ($N_s = 2^{22}$ total input signal samples) and 83% when $N_Q = 25$ total layers were available ($N_s = 2^{25}$ total input signal samples). Representative average computing times are shown in Table 5.1

Table 5.1 Average Layer Computing Time

Layer #	C.T. (min)	Layer #	C.T. (min)	Layer #	C.T. (min)	Layer #	C.T. (min)	Layer #	C.T. (min)
1	6	6	21	11	36	16	54	21	138
2	9	7	24	12	39	17	59	22	213
3	12	8	27	13	42	18	66	23	360
4	15	9	30	14	46	19	78	24	655
5	18	10	33	15	49	20	99	25	1242

2. *Output Matrix Q_N Formatting*

   After computing this measurable output data corresponding to Δt and Δf, sample frequency, signal amplitude (real or complex) or magnitude values were successfully save for further analysis and the results were consistent with studied input signals. As result of a given Q_N matrix a 2D F-T plot was computed which permitted to visually assess input signal characteristics such as bandwidth (W_{-30dB}), signal duration (T_s), time and frequency allocation.

3. *Time Resolution (Δt) Analysis*

   This output was used to ensure consistency between the average QMFB time vector extracted from a given Q_N matrix and the input signal time response. This was done using a 1D overlay plot of the averaged QMFB output response and the input signal's time response.

4. *Frequency Resolution (Δf) Analysis*

   This output was used to ensure consistency between the average QMFB frequency vector extracted from a given Q_N matrix and the input signal frequency domain (PSD) response. This was done using a 1D overlay plot of the averaged QMFB output response and the input signal's PSD response.

After evaluating the overall performance of the QMFB process with the signals of interest, it can be concluded that it is possible to perform reliable qualitative visual assessment of OFDM-based signals. Using this passive method some distinctive signal

parameters can be extracted such as bandwidth (W), center frequency (f_c), signal duration (T_s), frequency content and time allocation.

Related to the 802.11a Wi-Fi signal, the 10 short preamble symbols were successfully computed and results of the QMFB output matched the standard definition given in [9]. The guard interval between the preamble and the payload was also indentified using both single and integrated burst inputs. After performing burst integration, the QMFB output visually matched the expected results using 2D F-T plots, with lower energy observed in the data payload region due to random symbol assignment.

Related to the 802.16e WiMAX signal, the single burst *range-only* and *data-only* responses were successfully processed and matched the standard definition given in [12]. Even though presenting noise-like signal behavior in the 2D F-T plots, QMFB responses for both cased were sufficient to note differences in frequency and time allocations. Responses using integrated burst inputs were similar as those computed for the 802.11a Wi-Fi signal. Key signal features of center frequency (f_c), frequency content and time allocation were easily extractable. With further layer analysis, approximations to symbol duration (T_s) and bandwidth (W) were available as well.

The main research objective was met and the QMFB process presents an acceptable response for extracting some key features from 802.011a Wi-Fi and 802.16e WiMAX signals. This empirical approach permitted exploitation of OFDM-based signals using qualitative visual assessment such as may benefit human analysts.

5.3 Recommendations for Future Research

Further exploitation of the passive QMFB process should be considered in future

work based on different QMFB modification and decompositions. Benefit may be realized using QMFB processing aimed to accomplish automatic signal detection, channel estimation or signal fingerprinting analysis. Some specific future research activities could include:

1. *OFDM-Based Signal Detection Using Correlation Methods*

   Create a signal data base according to IEEE standard definitions for specific signals. Simulated data base features could be correlated with experimental QMFB exploited features with a goal of finding distinctive characteristics.

2. *RF Signal Fingerprinting Using QMFB Features*

   Assess the use of experimental 2D QMFB (complex or real) outputs to generate features for discriminating between signals from different devices using RF fingerprints. This process has been previously demonstrated using 2D Gabor Transform (GT) features [0, 11] and could be considered for expanding the applicability of QMFB processing.

3. *Compare 2D QMFB Outputs with Other 2D Transform Outputs*

   Improved signal exploitation may be possible using different 2D transforms, e.g., Gabor-based [0, 11]. Performance and computation time could be compared with QMFB processing as implemented here.

4. *Consider G-M Transformed QMFB Processing*

   Detection and estimation may be improved using QMFB outputs and transformation methods investigated previously by [4] which used the Grohholz-Mims (G-M) 2D transformation methods for non-cooperative

multi-channel detection [5, 6]. These methods have not been applied to OFDM-based signals such as done here with QMFB processing and results in [4] suggests that G-M transformed QMFB processing may be well-suited for additional investigation.

APPENDIX A – Simulation Code

This appendix presents the implemented MATLAB® code according to the adopted methodology and the defined measurable outputs.

A.1 Time and Frequency Input Signal Responses

```
% Original file: SigPSD_V2 Function
% Created by:    Dr. Michael A. Temple
% Modified by:   Felipe E. Garrido, CAP. Chilean Air Force
% Last update:   02/16/2012
%
% ====================== SigPSD_V3 Function ==========================
%
%   function [SigPsd,Fscale,SigPow] =
%       SigPSD_V3(SigIn,Fsamp,SAve,NAve,SNorm,SPlot,t_lim,f_lim,dB_lim)
%
%   Calculates Row-Wise Power Spectral Density (PSD) as the Magnitude
%   of Fourier Transform Coefficients Squared.  Resultant PSD (SigPsd)
%   and Average Power Estimate (SigPow) are output.
%
%   Created:  Apr 06, MAT
%   Modified: 19 Apr 11, MAT .. Enable Matrix Input/Output
%   Modified: 7 Sep 11, MAT ... Minor Change to Plotting Output
%   Modified: 14 Dec 11, MAT .. Save time and frequency responses as
%                               vector.
%
%   NOTE:  Outputs Verified/Consistent with Matlab's 'PSD' Function for
%          BOTH Complex and Real-Valued Input Signal (10 Dec 08).
%
%   Inputs:
%   SigIn   Nrow x NCol Matrix: NCol = Time Domain Signal Samples
%   Fsamp   Sample Frequency (Samples/Sec)
%   SAve    PSD Averaging Control Variable (Sliding Window Average)
%           (1 = Average Applied, 0 = No Average Applied)
%   NAve    Number of Points Averaged Across
%           (Odd Number Required if Save = 1, Else, Doesn't Matter)
%   SNorm   Normalization Control Variable
%           (1 = Normalized, 0 = UnNormalized)
%   SPlot   Plot Control Variable (1 = Plot, 0 = No Plot).  Two plots
%           are generated for SPlot=1: A) Time Domain Waveform
%           (amplitude for SigIn Real and Magnitude for SigIn Complex),
%           B) SigIn PSD (spanning -Fsamp/2 < f < Fsamp/2 for SigIn
%           Real and 0 < f < Fsamp for SigIn Complex).
%   t_lim   Time window = to plot time response [0,t_lim]
%   f_lim   Frequency window = to plot frequency response [0,f_lim]
%   dB_lim  Magnitude window = Defines min dB level to plot [dB_lim,0]
%
%   Outputs:
%   SigPsd  PSD of Input Signal Calc as |Fourier{SigIn}|^2
%   Fscale  Resultant Frequency Scale for Output PSD
%   SigPow  Estimated Power Estimate Calc as Sum of PSD Components
% ====================================================================
```

```
function [SigPsd,Fscale,SigPow] =
SigPSD_V3(SigIn,Fsamp,SAve,NAve,SNorm,SPlot,t_lim,f_lim,dB_lim)

[NrowIn,NcolIn]=size(SigIn);

if NcolIn==1 % Column Vector Input  Transpose & Process as Row Vector
    SigIn=SigIn.';
    [Nrow,Ncol]=size(SigIn);
else
    Nrow=NrowIn;
    Ncol=NcolIn;
end

SigVal = isreal(SigIn(1,1)); % SigVal=1 (Real) or SigVal=0 (Complex)

SigFFT=(fft(real(SigIn.')).'/Ncol);
SigPsd=abs(SigFFT).^2; % Non-Shifted PSD

SigPow=sum(SigPsd.');

if(SAve==1) % Apply Row-Wise Averaging/Smoothing to PSD
    NTest = mod(NAve,2); % Check/Adjust NAve to be an Odd Number
    if NTest==0 % Even NAve Input
        NAve=NAve+1; % Adjust NAve to be Odd
    end;
    for j=1:Nrow
        %TmpPsd=SigPsd(j,:);
        SigPsd(j,:)=smooth(SigPsd(j,:),NAve);
    end
end

PSDmax=max(SigPsd.');
PSDfloor=PSDmax/10000; % Set PSD Floor Level to -40 dB Below Max Value

for j=1:Nrow % Threshold / Set PSD Floor Values
    for k=1:Ncol
        if SigPsd(j,k)<PSDfloor(j)
            SigPsd(j,k)=PSDfloor(j);
        end
    end
end

PSDmax=max(SigPsd.'); % Update PSDmax
if SNorm==1 % Normalize PSD if Selected
    SigPsd=SigPsd./repmat(PSDmax.',1,Ncol);
end

if NcolIn==1 % Return Output to Column Vector
    SigPsd=SigPsd.';
end

delf=Fsamp/(Ncol-1); % Freq Plot Step Size
Fscale=0:delf:(Ncol-1)*delf; % Output PSD Freq Scale

if SPlot==1 % Produce Output Plots

    disp(' ')
    disp('Generating Plot')
    disp(' ')
```

```
    if (Nrow==1||Ncol==1 )
        SigPlot=(abs(SigIn)).^2;
        SigPlot=SigPlot/max(SigPlot);
        PsdPlot=SigPsd;
    else % Use 1st Row of SigIn & SigPsd Matrix for Plot Default
        SigPlot=(abs(SigIn(1,:))).^2;
        PsdPlot=SigPsd(1,:);
    end

    figure
    subplot(2,1,1) % Top Time Plot
    tscale=linspace(0,Ncol/Fsamp,Ncol);
    SigPlot_dB=10*log10(SigPlot);

    if SigVal==1 % SigIn is Real
        plot(tscale,SigPlot_dB);
        grid;
        set(gca,'XLim',[0 t_lim]);
        set(gca,'YLim',[dB_lim 0]);
        xlabel('Time [s]')
        ylabel('Magnitude')
    else % SigIn is Complex ... Plot Amplitude as Abs(SigIn)
        plot(tscale,SigPlot_dB);
        grid;
        set(gca,'XLim',[0 t_lim]);
        set(gca,'YLim',[dB_lim 0]);
        xlabel('Time [s]')
        ylabel('Magnitude')
    end

    save('Time_response','SigPlot_dB','tscale');

    subplot(2,1,2) % Select Middle PSD Figure

    if SigVal==1 % SigIn Real: Plot FFTshift{PSD} for -Fs/2 < f < Fs/2
        fpos=(0:delf:delf*(ceil(Ncol/2)-1));
        fneg= -fliplr( (delf:delf:delf*(Ncol-ceil(Ncol/2))) );
        FrqPlot=[fneg fpos];
        FrqPlot_dB=10*log10(fftshift(PsdPlot));
        plot(FrqPlot,FrqPlot_dB); % PSD Shifted

    else % SigIn Complex: Plot PSD for 0 < f < Fsamp
        FrqPlot=0:delf:(Ncol-1)*delf;
        FrqPlot_dB=10*log10(PsdPlot);
        plot(FrqPlot, FrqPlot_dB); % FFT Shifted

    end

    save('PSD_signal','FrqPlot_dB','FrqPlot');

    % Adjust X & Y Axis Limits
    set(gca,'YLim',[dB_lim 0]);
    set(gca,'XLim',[0 f_lim]);
    xlabel('Frequency [Hz]')
    ylabel('| FFT |^ 2')
    grid
end
% ====================== End SigPSD_V3 Function======================
```

A.2 QMFB Process Code

```
% QMFB PROCESS
% Original file: qmfb.m
% Created by   : Phillip E. Pace
% Modified by  : Felipe Garrido, CAP. Chilean Air Force.
% Last update  : 02/02/2012.
% This code is used to create the layers and the neccesary output data
% to processing them according to the desired time-frequency plot
% This code call the function tsinc.m that creates de coefficients
% according to the especified filter created for Phillip E. Pace.
%%%%%%%%%%%%%%%%%%%%%%%%%%%%%%%%%%%%%%%%%%%%%%%%%%%%%%%%%%%%%%%%%%%%%%%%%%%%%%%%
clear all
close all
tic
% Files Loading
load preamble_res_10000_25.mat
% -- Input data --
c0=[preamble_res_10000_25]';  % Input signal padded with zeros
[d1, c1] = tsinc(c0);    % Sinc Modified Filter function
% -- Number of Layers to Compute --
f=c0;                         % Input signal
n = floor(log2(length(f)));  % Determine the amount of layers from the length
of the signal
N = n;                        % number of layers
% -- Formatting the Signal -- (to pass the signal through the filter bank)
I(1:2^n,1) = f(1:2^n);
out = I;

% -- Generating the Output Layers --

% Decompose the function
W = waitbar(0,'Computing Layers...');
for lay = 1:N    % layer
  %disp(lay)     % Show what layer is been generated
  waitbar(lay/(N+1),W)
  flag = 1;     % Flag used to set up the columns in the output matrix

  % Reshape the output matrix
  [r,c] = size(out);
  out = zeros(r./2, c.*2);

  for i = 1:2 ^(lay-1)         % column of I (low to high)
    [G,H] = tsinc(I(:,i));     % Evaluate the filter (sinc modified)
                               % over the signal going by columns

    % Setting the output matrix (Layer) by High Pass (G) and Low Pass (H)
filtering output
    if flag
        out(:, i.*2-1) = H;    % Low Pass Branch of QMFB Tree
        out(:, i.*2) = G;      % High Pass Branch of QMFB Tree
    else
        out(:, i.*2-1) = G;    % High Pass Branch of QMFB Tree
        out(:, i.*2) = H;      % Low Pass Branch of QMFB Tree
    end;
        flag = ~flag;          % Change in the flag value
  end;

  % Output Matrix and data to work with
```

```
  I = out;         % Output matrix (signal already filtered)
  R = real(I);     % Real part of the filtered signal
  Q = imag(I);     % Imaginary part of the filtered signal

  % Saving the data to the same directory
  save(['layer',int2str(lay)],'R','Q');
end;
close (W)
toc
%=====================End of QMFB Process=================================

function [d1, c1] = tsinc(c0)   % Sinc Modified Filter function

% [d1, c1] = tsinc(c0)
% Sinc Modified Filter function. It use truncated sinc modified filter
% coefficients to decompose the column vector c0 into a (high frequency)
% column vector d1 and (low frequency) column vector c1.
%=========================================================================
% -- Sinc Modified Filter Formula Application --
N = 512; % Number of filters coefficients pairs.
C = 1.99375872328059; % Value to get cross corr of less than   0.001
S = 1.00618488680080; % Value to get cross corr of less than 0.001
x = (-floor(N./2):(floor(N./2)-1))'; % Vector coefficients
h = sqrt(S./2).*sinc((x + .5)./C); % Coefficients filter formula
w = hamming(N); % Hamming Window
h = w.*h; % Low Pass Filter Coefficients
g = h; % High Pass Filter Coefficients
g(2:2:N) = -h(2:2:N); % Alternating the sign of the coefficients
%=========================================================================
% -- Setting the Signal --
N = length(c0);              % Length of the signal
%                              (from qmfb function "c0" is a column)
pad3 = length(h)./2 + 1;     % pad with zeros to clear out filter
c0 = [c0; zeros(pad3,1)];    % padding with zeros
%=========================================================================
% Decompose the column vector c0
i = pad3:2:(N+pad3-2);               % i will decimate by 2

% c1 low frequency column vector
c1 = filter(fliplr(h),1,c0);         % compute c1
c1 = c1(i);                          % decimate

% d1 high frequency column vector d1
d1 = filter(fliplr(g),1,c0);         % compute d1
d1 = d1(i);                          % decimate
%=========================================================================
```

A.3 Q_N Matrix Generation Code

```
% Qn Matrix generation and Plotting
% Original file  : qmfb.m
% Created by     : Phillip E. Pace
% modified by    : Capt Felipe E. Garrido 01/04/2012
% Last update    : 02/16/2012
%%%%%%%%%%%%%%%%%%%%%%%%%%%%%%%%%%%%%%%%%%%%%%%%%%%%%%%%%%%%%%%%%%%%%%%%%%%%
% This code allows to choose which layers do you want to plot
% and save the matrix with useful data as Q_xx.mat,xx= layer number
%
% Input variables are the following:
% L= lower layer to plot (Min layer=1)
% H= higher layer to plot (Max layer= N)
% fs= Sampling frequency of the input data (Fsamp_XX)
% freq_limit= max frequency in window
% Time_limit= max time in window
%%%%%%%%%%%%%%%%%%%%%%%%%%%%%%%%%%%%%%%%%%%%%%%%%%%%%%%%%%%%%%%%%%%%%%%%%%%%
clear all
close all
%% Warning:
% Check you are loading the correct data file
load preamble_res_10000_25.mat;

%% Set the appropiate parameters

fs=Fsamp_10000;         % Sample frequency according to the
                        % resampled data
L=2;                    % Lower layer to plot
H=24;                   % Higher layer to plot
freq_limit=9e6;         % Y axis limit
Time_limit=2.5e-5;      % X axis limit


%% Plotting
for yy=L:H

    load (['layer',num2str(yy),'.mat']);
    % Formating the Layer
    layer = abs(R + 1i*Q);              % absolute value of the layer
    layer = (layer/max(max(layer))).^2;% Normalizing the layer
    M = layer;                          % Set values to dB
    [m,n]=size(M);                      % Set axis sizes
    T=1/fs;                             % Sampling period
    f=linspace(0,fs/2,n);               % Setting the frequency axis
    NUM_SAMPLES = m*n;                  % Length of the new signal
    time=linspace(0,NUM_SAMPLES*T,m);  % Setting the time axis
    dt=(NUM_SAMPLES*T)/(m-1);           % delta t
    df=(fs/(2*(n-1)));                  % delta f

    t_max=ceil(Time_limit/dt)+1;
    f_max=ceil(freq_limit/df)+1;

    new_Q=(M(1:(t_max),1:(f_max))).';
    new_layer=(R(1:(t_max),1:(f_max)) + 1i*Q(1:(t_max),1:(f_max))).';
    n_t=time(1:t_max);
    n_f=f(1:f_max);
    Q_dB=10*log10(new_Q.^2);
```

```
    clear layer;        % clear current layer matrix from the workspace

    % Color Plots
    figure;
    %pcolor(time(1:t_max),f(1:f_max),Q_dB')
    pcolor(n_t,n_f,Q_dB)
%     title(['"Time - Frequency Plane Layer ',...
%            num2str(yy),' with   \Deltat=',num2str(dt),...
%            ' and  \Deltaf=',num2str(df),'"'])
    xlabel('Time [s]'),ylabel('Frequency [Hz]')
    colorbar,colormap(jet)
    caxis([-30,0])
    shading interp

%     figure;
%     %pcolor(time(1:t_max),f(1:f_max),Q_dB')
%     pcolor(n_t,n_f,Q_dB)
% %      title(['"Time - Frequency Plane Layer ',...
% %            num2str(yy),' with   \Deltat=',num2str(dt),...
% %            ' and  \Deltaf=',num2str(df),'"'])
%     xlabel('Time [sec]'),ylabel('Frequency [Hz]')
%     colorbar,colormap(jet)
%     caxis([-30,0])
%     shading flat

    save(['Q_',int2str(yy)],'Q_dB','new_Q','time','f','dt','df',...
         'fs','t_max','f_max','new_layer');
end
```

A.4 Input/Output Frequency-Time (F-T) Analysis Code

```
% TIME AND FREQUENCY ANALYSIS
%
% Created by  : Felipe E. Garrido, CAP. Chilean Air Force
% Last update : 02/16/2012
%
% This code computes and save Normalized Average Time
% and Normalized Average frequency vector for a given layer
%
%%%%%%%%%%%%%%%%%%%%%%%%%%%%%%%%%%%%%%%%%%%%%%%%%%%%%%%%%%%%%%%%%%%%%%%%%%%%%%%
%% Warning
% 1.- The file Layer_plotting, must be run before running this code to
%     generate a given Q_XX.mat file.
%
%%%%%%%%%%%%%%%%%%%%%%%%%%%%%%%%%%%%%%%%%%%%%%%%%%%%%%%%%%%%%%%%%%%%%%%%%%%%%%%
%%
% Input variables are the following:
% layer = number of the layer you want to plot (Min layer=1)
% sel   = variable to choose between time or frequency
% Choose:
% Time plot      ===> sel=1
% Frequency plot ===> sel=2
%
%%%%%%%%%%%%%%%%%%%%%%%%%%%%%%%%%%%%%%%%%%%%%%%%%%%%%%%%%%%%%%%%%%%%%%%%%%%%%%%

clear all
close all

layer=13;                  % Choose the layer to plot
load (['Q_',num2str(layer),'.mat']);


sel=1;                     % Time plot=1, Frequency plot=2

%     n_t=time(1:t_max);
%     n_f=f(1:f_max);
%     Q_dB=10*log10(new_Q.^2);

if sel==1;
    t=mean(new_Q,1);
    t2=t/max(t);
    t2_dB=10*log10(t2(1:t_max));
    tt=time(1:t_max);
    figure;
    plot(tt,t2_dB)
%     title(['"Normalized Average Time plot for Layer ',...
%            num2str(layer),' with   \Deltat=',num2str(dt),'"'])
    %xlabel('Time [s]')
    ylabel('dB')
    ylim([-30 0])
    xlim([0 Time_limit])
    grid on

    save(['ave_t_',int2str(layer)],'t2_dB','tt');

elseif sel==2;
    nf=mean(new_Q,2);
    f2=nf/max(nf);
```

```
    f2_dB=10*log10(f2(1:f_max));
    w=f(1:f_max);
    figure;
    plot(f2_dB,w)
%     title(['"Normalized Average frequency plot for Layer ',...
%            num2str(layer),' with   \Deltaf=',num2str(df),'"'])
    %ylabel('Frequency [Hz]')
    xlabel('dB')
    xlim([-30 0])
    ylim([0 freq_limit])
    grid on

    save(['ave_f_',int2str(layer)],'f2_dB','w');

else
    disp('ERROR:')
    disp('Choose: 1=Plot Average Time or 2=Plot Average Frequency')
end
%=====================End of Time/Frequency analysis code====================


% OVERLAY FREQUENCY RESPONSE PLOT
%
% Created by  : Felipe E. Garrido, CAP. Chilean Air Force
% Last update : 02/16/2012
%
% This code computes overlay frequency response according to input
% signal and two chosen layers
%
%%%%%%%%%%%%%%%%%%%%%%%%%%%%%%%%%%%%%%%%%%%%%%%%%%%%%%%%%%%%%%%%%%%%%%%%%%%%
% Input variables are the following:
% PSD_signal.mat = initial signal frequency response
% ave_f_20.mat   = single burst frequency response
% ave_f_19.mat   = burst integration frequency response
%%%%%%%%%%%%%%%%%%%%%%%%%%%%%%%%%%%%%%%%%%%%%%%%%%%%%%%%%%%%%%%%%%%%%%%%%%%%

clear all
close all

load PSD_signal.mat
figure
plot (FrqPlot,FrqPlot_dB,'b')
hold on

load ave_f_20.mat
plot(w,f2_dB,'r')

hold on
load ave_f_19.mat
plot(w,f2_dB,'k')

grid on
legend('Input','Single Burst','Burst Integration','location','South')
xlim([0 2e6])
ylim([-30 0])
xlabel('Frequency [Hz]')
ylabel('Magnitude [dB]')

%=====================End of Overlay FREQUENCY response======================
```

```
% OVERLAY TIME RESPONSE PLOT
%
% Created by  : Felipe E. Garrido, CAP. Chilean Air Force
% Last update : 02/16/2012
%
% This code computes overlay frequency response according to input
% signal and two chosen layers
%
%%%%%%%%%%%%%%%%%%%%%%%%%%%%%%%%%%%%%%%%%%%%%%%%%%%%%%%%%%%%%%%%%%%%%%%%%%%%%%%
% Input variables are the following:
% Time_response.mat = initial signal frequency response
% ave_t_13.mat   = single burst frequency response
% ave_t_12.mat   = burst integration frequency response
%%%%%%%%%%%%%%%%%%%%%%%%%%%%%%%%%%%%%%%%%%%%%%%%%%%%%%%%%%%%%%%%%%%%%%%%%%%%%%%


clear all
close all

load Time_response.mat
figure
plot (tscale,SigPlot_dB,'b')
hold on

load ave_t_13.mat
plot(tt,t2_dB,'r')

hold on
load ave_t_12.mat
plot(tt,t2_dB,'k')

grid on
legend('Input','Single Burst','Burst Integration','location','south')
xlim([0 0.1e-3])
ylim([-30 0])
xlabel('Time [s]')
ylabel('Magnitude [dB]')

%=====================End of Overlay TIME response======================
```

APPENDIX B – QMFB Outputs for 802.11a Wi-Fi Preamble Signal

This appendix presents a complete set of available layer outputs (Q_N) for the 802.11a signal analyzed in Section 4.2 according to computed QMFB outputs.

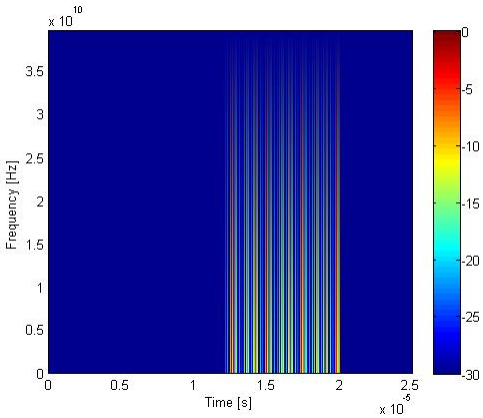

QMFB Layer Q_2

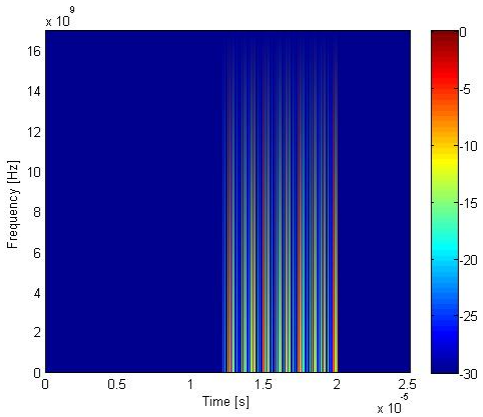

QMFB Layer Q_3

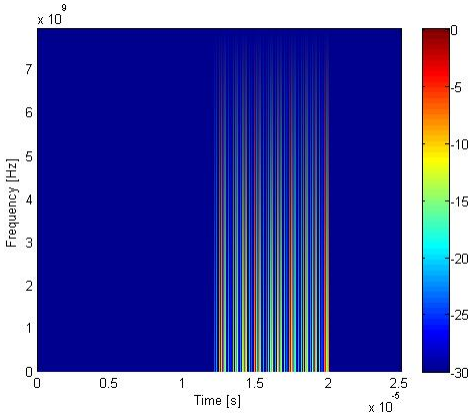

QMFB Layer Q_4

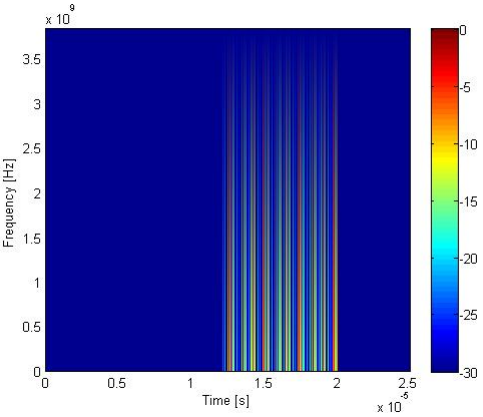

QMFB Layer Q_5

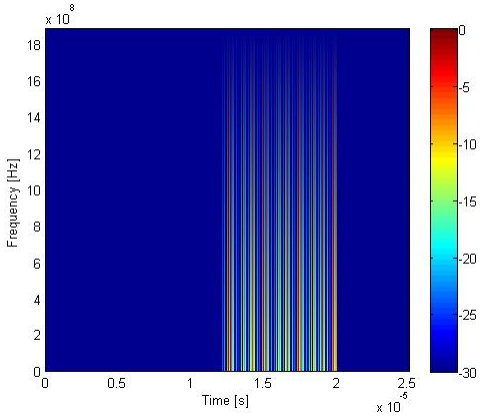

QMFB Layer Q_6

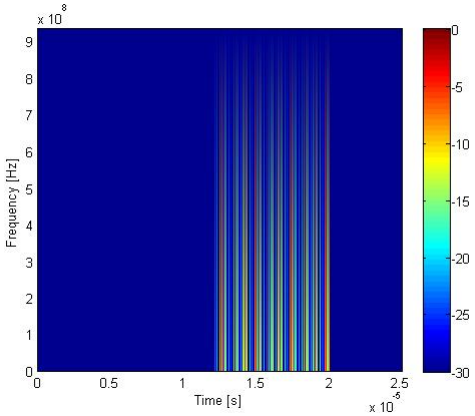

QMFB Layer Q_7

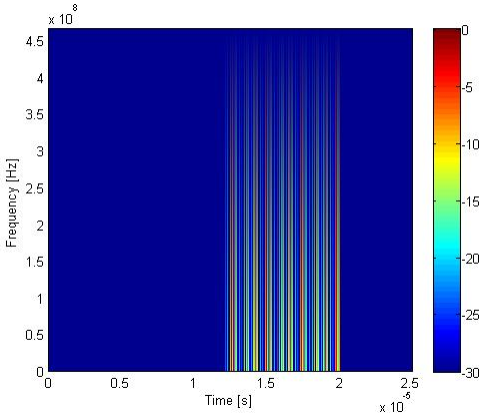

QMFB Layer Q_8

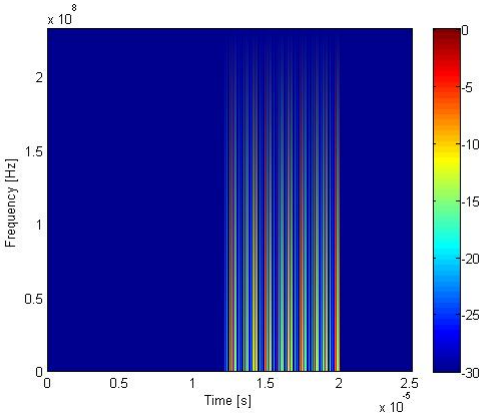

QMFB Layer Q_9

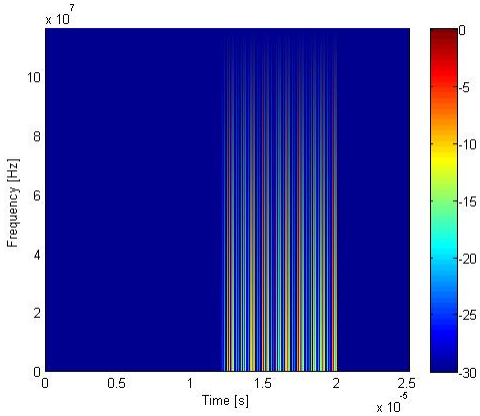

QMFB Layer Q_{10}

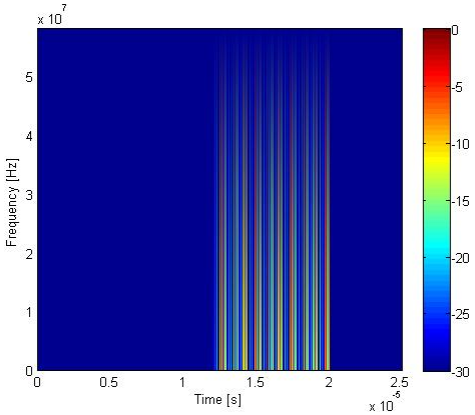

QMFB Layer Q_{11}

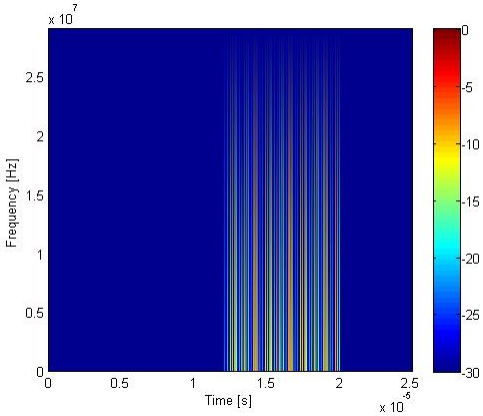

QMFB Layer Q_{12}

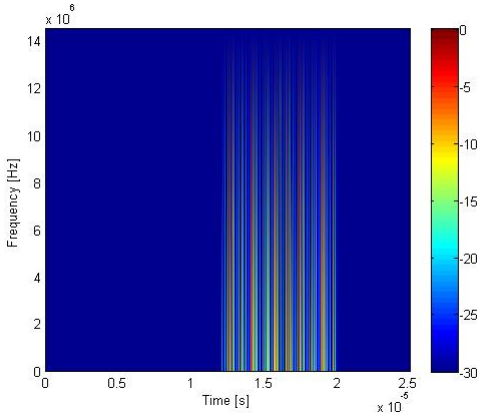

QMFB Layer Q_{13}

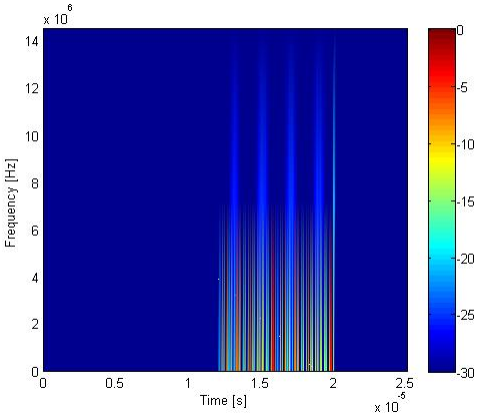

QMFB Layer Q_{14}

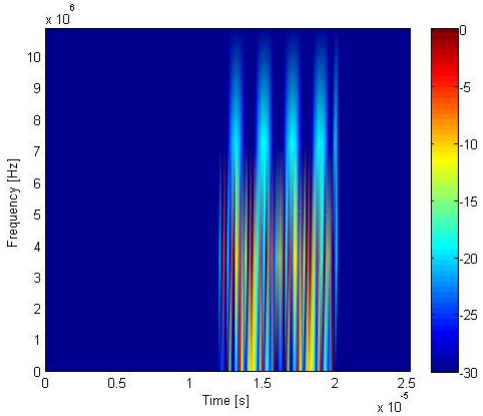

QMFB Layer Q_{15}

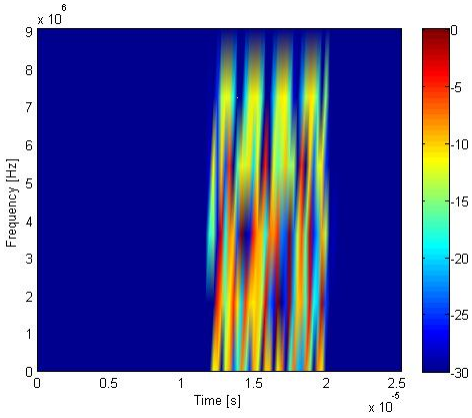

QMFB Layer Q_{16}

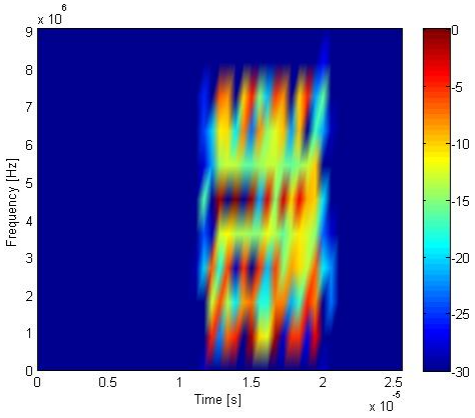

QMFB Layer Q_{17}

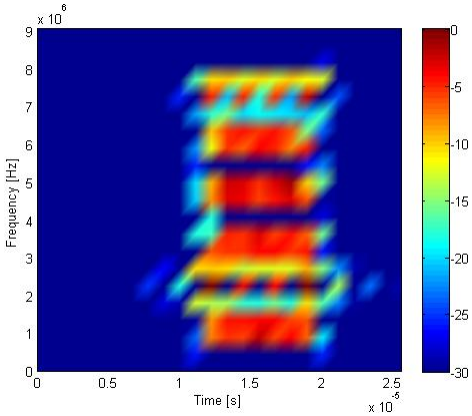

QMFB Layer Q_{18}

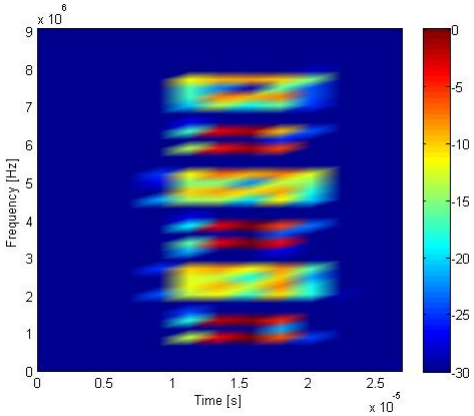

QMFB Layer Q_{19}

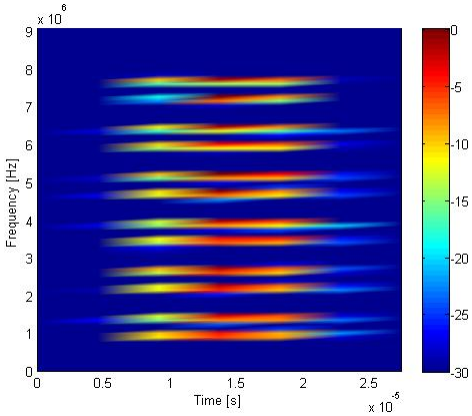

QMFB Layer Q_{20}

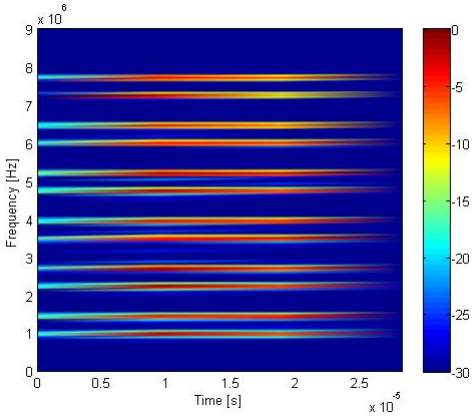

QMFB Layer Q_{21}

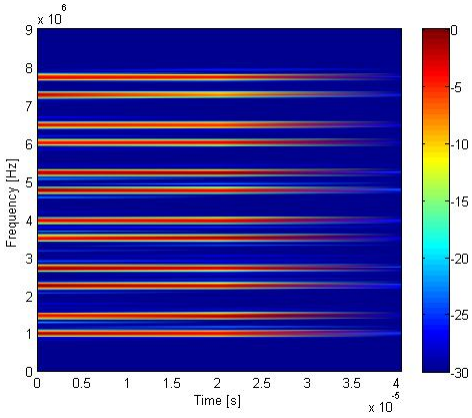

QMFB Layer Q_{22}

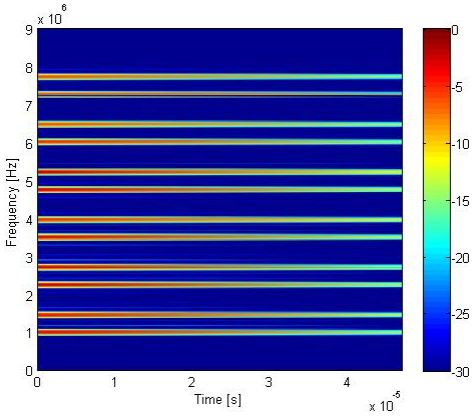

QMFB Layer Q_{23}

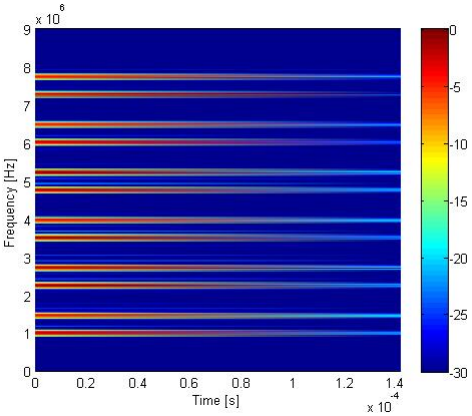

QMFB Layer Q_{24}

APPENDIX C. Time (Δt) and Frequency (Δf) Resolution Tables

C.1 802.11a Wi-Fi Signal: Preamble Only (Section 4.2.1)

Sampling Frequency f_s [Hz]	$f_s = 5.94\text{x}10^{10}$		$f_s = 1.19\text{x}10^{11}$		$f_s = 2.38\ \text{x}10^{11}$	
Layer #	Δf [Hz]	Δt [s]	Δf [Hz]	Δt [s]	Δf [Hz]	Δt [s]
6	$4.71\text{x}10^{8}$	$1.08\text{x}10^{-9}$	$9.43\text{x}10^{8}$	$5.39\text{x}10^{-10}$	$1.89\text{x}10^{9}$	$2.70\text{x}10^{-10}$
7	$2.33\text{x}10^{8}$	$2.16\text{x}10^{-9}$	$4.68\text{x}10^{8}$	$1.08\text{x}10^{-9}$	$9.35\text{x}10^{8}$	$5.39\text{x}10^{-10}$
8	$1.16\text{x}10^{8}$	$4.31\text{x}10^{-9}$	$2.33\text{x}10^{8}$	$2.16\text{x}10^{-9}$	$4.66\text{x}10^{8}$	$1.08\text{x}10^{-9}$
9	$5.81\text{x}10^{7}$	$8.62\text{x}10^{-9}$	$1.16\text{x}10^{8}$	$4.31\text{x}10^{-9}$	$2.32\text{x}10^{8}$	$2.16\text{x}10^{-9}$
10	$2.90\text{x}10^{7}$	$1.73\text{x}10^{-8}$	$5.80\text{x}10^{7}$	$8.62\text{x}10^{-9}$	$1.16\text{x}10^{8}$	$4.31\text{x}10^{-9}$
11	$1.45\text{x}10^{7}$	$3.45\text{x}10^{-8}$	$2.90\text{x}10^{7}$	$1.73\text{x}10^{-8}$	$5.80\text{x}10^{7}$	$8.62\text{x}10^{-9}$
12	$7.25\text{x}10^{6}$	$6.90\text{x}10^{-8}$	$1.45\text{x}10^{7}$	$3.45\text{x}10^{-8}$	$2.90\text{x}10^{7}$	$1.73\text{x}10^{-8}$
13	$3.62\text{x}10^{6}$	$1.38\text{x}10^{-7}$	$7.25\text{x}10^{6}$	$6.90\text{x}10^{-8}$	$1.45\text{x}10^{7}$	$3.45\text{x}10^{-8}$
14	$1.81\text{x}10^{6}$	$2.76\text{x}10^{-7}$	$3.62\text{x}10^{6}$	$1.38\text{x}10^{-7}$	$7.25\text{x}10^{6}$	$6.90\text{x}10^{-8}$
15	$9.06\text{x}10^{5}$	$5.52\text{x}10^{-7}$	$1.81\text{x}10^{6}$	$2.76\text{x}10^{-7}$	$3.62\text{x}10^{6}$	$1.38\text{x}10^{-7}$
16	$4.53\text{x}10^{5}$	$1.11\text{x}10^{-6}$	$9.06\text{x}10^{5}$	$5.53\text{x}10^{-7}$	$1.81\text{x}10^{6}$	$2.77\text{x}10^{-7}$
17	$2.27\text{x}10^{5}$	$2.22\text{x}10^{-6}$	$4.53\text{x}10^{5}$	$1.11\text{x}10^{-6}$	$9.06\text{x}10^{5}$	$5.56\text{x}10^{-7}$
18	$1.13\text{x}10^{5}$	$4.45\text{x}10^{-6}$	$2.26\text{x}10^{5}$	$2.23\text{x}10^{-6}$	$4.53\text{x}10^{5}$	$1.11\text{x}10^{-6}$
19	$5.66\text{x}10^{4}$	$8.97\text{x}10^{-6}$	$1.13\text{x}10^{5}$	$4.49\text{x}10^{-6}$	$2.27\text{x}10^{5}$	$2.25\text{x}10^{-6}$
20	$2.83\text{x}10^{4}$	$1.82\text{x}10^{-5}$	$5.66\text{x}10^{4}$	$9.12\text{x}10^{-6}$	$1.13\text{x}10^{5}$	$4.56\text{x}10^{-6}$
21	$1.42\text{x}10^{4}$	$3.77\text{x}10^{-5}$	$2.83\text{x}10^{4}$	$1.88\text{x}10^{-5}$	$5.66\text{x}10^{4}$	$9.42\text{x}10^{-6}$

C.2 802.11a Wi-Fi Signal: Complete Burst (Section 4.2.2)

Sampling Frequency f_s [Hz]	$f_s = 2.38\text{x}10^{10}$		$f_s = 5.94\ \text{x}10^{10}$		$f_s = 1.31\ \text{x}10^{11}$	
Layer #	Δf [Hz]	Δt [s]	Δf [Hz]	Δt [s]	Δf [Hz]	Δt [s]
6	$1.88\text{x}10^{8}$	$2.69\text{x}10^{-9}$	$4.71\text{x}10^{8}$	$1.08\text{x}10^{-9}$	$1.04\text{x}10^{9}$	$4.90\text{x}10^{-10}$
7	$9.35\text{x}10^{7}$	$5.39\text{x}10^{-9}$	$2.33\text{x}10^{8}$	$2.16\text{x}10^{-9}$	$5.14\text{x}10^{8}$	$9.80\text{x}10^{-10}$
8	$4.66\text{x}10^{7}$	$1.08\text{x}10^{-8}$	$1.16\text{x}10^{8}$	$4.31\text{x}10^{-9}$	$2.56\text{x}10^{8}$	$1.96\text{x}10^{-9}$
9	$2.32\text{x}10^{7}$	$2.16\text{x}10^{-8}$	$5.81\text{x}10^{7}$	$8.62\text{x}10^{-9}$	$1.27\text{x}10^{8}$	$3.92\text{x}10^{-9}$
10	$1.15\text{x}10^{7}$	$4.31\text{x}10^{-8}$	$2.90\text{x}10^{7}$	$1.73\text{x}10^{-8}$	$6.38\text{x}10^{7}$	$7.84\text{x}10^{-9}$
11	$5.80\text{x}10^{6}$	$8.63\text{x}10^{-8}$	$1.45\text{x}10^{7}$	$3.45\text{x}10^{-8}$	$3.19\text{x}10^{7}$	$1.57\text{x}10^{-8}$
12	$2.89\text{x}10^{6}$	$1.73\text{x}10^{-7}$	$7.25\text{x}10^{6}$	$6.90\text{x}10^{-8}$	$1.59\text{x}10^{7}$	$3.14\text{x}10^{-8}$
13	$1.44\text{x}10^{6}$	$3.45\text{x}10^{-7}$	$3.62\text{x}10^{6}$	$1.38\text{x}10^{-7}$	$7.97\text{x}10^{6}$	$6.27\text{x}10^{-8}$
14	$7.25\text{x}10^{5}$	$6.93\text{x}10^{-7}$	$1.81\text{x}10^{6}$	$2.76\text{x}10^{-7}$	$3.99\text{x}10^{6}$	$1.25\text{x}10^{-7}$
15	$3.62\text{x}10^{6}$	$1.39\text{x}10^{-6}$	$9.06\text{x}10^{5}$	$5.52\text{x}10^{-7}$	$1.99\text{x}10^{6}$	$2.51\text{x}10^{-7}$
16	$1.81\text{x}10^{5}$	$2.80\text{x}10^{-6}$	$4.53\text{x}10^{5}$	$1.11\text{x}10^{-6}$	$9.97\text{x}10^{6}$	$5.03\text{x}10^{-7}$
17	$9.06\text{x}10^{4}$	$5.70\text{x}10^{-6}$	$2.27\text{x}10^{5}$	$2.22\text{x}10^{-6}$	$4.98\text{x}10^{5}$	$1.01\text{x}10^{-6}$
18	$4.53\text{x}10^{4}$	$1.18\text{x}10^{-5}$	$1.13\text{x}10^{5}$	$4.45\text{x}10^{-6}$	$2.49\text{x}10^{5}$	$2.02\text{x}10^{-6}$
19	$2.26\text{x}10^{4}$	$2.52\text{x}10^{-5}$	$5.66\text{x}10^{4}$	$8.97\text{x}10^{-6}$	$1.25\text{x}10^{5}$	$4.08\text{x}10^{-6}$
20	$1.13\text{x}10^{4}$	$5.89\text{x}10^{-5}$	$2.83\text{x}10^{4}$	$1.82\text{x}10^{-5}$	$6.23\text{x}10^{4}$	$8.29\text{x}10^{-6}$
21	$5.63\text{x}10^{3}$	$1.21\text{x}10^{-4}$	$1.42\text{x}10^{4}$	$3.77\text{x}10^{-5}$	$3.11\text{x}10^{4}$	$1.71\text{x}10^{-5}$

C.3 802.16e WiMAX Signal

Sampling Frequency f_s [Hz]	Both Modes $f_s = 1.19\text{x}10^9$		Data-Only $f_s = 1.18\text{x}10^{10}$		Range-Only $f_s = 3.56\ \text{x}10^{10}$	
Layer #	Δf [Hz]	Δt [s]	Δf [Hz]	Δt [s]	Δf [Hz]	Δt [s]
6	$9.42\text{x}10^{6}$	$5.39\text{x}10^{-8}$	$9.42\text{x}10^{7}$	$5.39\text{x}10^{-9}$	$2.83\text{x}10^{8}$	$1.80\text{x}10^{-9}$
7	$4.68\text{x}10^{6}$	$1.08\text{x}10^{-7}$	$4.68\text{x}10^{7}$	$1.08\text{x}10^{-8}$	$1.40\text{x}10^{8}$	$3.59\text{x}10^{-9}$
8	$2.32\text{x}10^{6}$	$2.16\text{x}10^{-7}$	$3.33\text{x}10^{7}$	$2.16\text{x}10^{-8}$	$6.99\text{x}10^{7}$	$7.19\text{x}10^{-9}$
9	$1.15\text{x}10^{6}$	$4.31\text{x}10^{-7}$	$1.16\text{x}10^{7}$	$4.31\text{x}10^{-8}$	$3.49\text{x}10^{7}$	$1.44\text{x}10^{-8}$
10	$5.80\text{x}10^{5}$	$8.62\text{x}10^{-7}$	$5.80\text{x}10^{6}$	$8.62\text{x}10^{-8}$	$1.74\text{x}10^{7}$	$2.87\text{x}10^{-8}$
11	$2.90\text{x}10^{5}$	$1.72\text{x}10^{-6}$	$2.90\text{x}10^{6}$	$1.72\text{x}10^{-7}$	$8.70\text{x}10^{6}$	$5.75\text{x}10^{-8}$
12	$1.45\text{x}10^{5}$	$3.45\text{x}10^{-6}$	$1.45\text{x}10^{6}$	$3.45\text{x}10^{-7}$	$4.34\text{x}10^{6}$	$1.15\text{x}10^{-7}$
13	$7.24\text{x}10^{4}$	$6.90\text{x}10^{-6}$	$7.25\text{x}10^{5}$	$6.90\text{x}10^{-7}$	$2.16\text{x}10^{6}$	$2.31\text{x}10^{-7}$
14	$3.62\text{x}10^{4}$	$1.38\text{x}10^{-5}$	$3.62\text{x}10^{5}$	$1.38\text{x}10^{-6}$	$1.09\text{x}10^{6}$	$4.60\text{x}10^{-7}$
15	$1.81\text{x}10^{4}$	$2.76\text{x}10^{-5}$	$1.81\text{x}10^{5}$	$2.76\text{x}10^{-6}$	$5.44\text{x}10^{5}$	$9.21\text{x}10^{-7}$
16	$9.06\text{x}10^{3}$	$5.53\text{x}10^{-5}$	$9.06\text{x}10^{4}$	$5.53\text{x}10^{-6}$	$2.71\text{x}10^{5}$	$1.84\text{x}10^{-6}$
17	$4.53\text{x}10^{3}$	$1.11\text{x}10^{-4}$	$4.53\text{x}10^{4}$	$1.11\text{x}10^{-5}$	$1.36\text{x}10^{5}$	$3.69\text{x}10^{-6}$
18	$2.27\text{x}10^{3}$	$2.33\text{x}10^{-4}$	$2.27\text{x}10^{4}$	$2.22\text{x}10^{-5}$	$6.80\text{x}10^{4}$	$7.42\text{x}10^{-6}$
19	$1.13\text{x}10^{2}$	$4.75\text{x}10^{-4}$	$1.13\text{x}10^{4}$	$4.45\text{x}10^{-5}$	$3.39\text{x}10^{4}$	$1.50\text{x}10^{-5}$
20	$5.63\text{x}10^{1}$	$1.02\text{x}10^{-3}$	$5.66\text{x}10^{3}$	$8.97\text{x}10^{-5}$	$1.69\text{x}10^{4}$	$3.03\text{x}10^{-5}$
21	$2.84\text{x}10^{1}$	$2.11\text{x}10^{-3}$	$2.83\text{x}10^{3}$	$1.82\text{x}10^{-4}$	$8.58\text{x}10^{3}$	$6.04\text{x}10^{-5}$

Bibliography

1. Pace, P. E. *Detecting and Classifying Low Probability of Intercept Radar*. Artech House, Boston, second edition, 2008. ISBN 978-1-59693-234.

2. Skelar, B. *Digital Communications Fundamentals and Applications*. Prentice Hall PTR, New Jersey, Second Edition, 2008. ISBN 0-13-084788-7.

3. Jarpa, P. *Quantifying the Differences in Low Probability of Intercept Radar Waveforms Using Quadrature Mirror Filtering*. Master's thesis, Naval Postgraduate School, Monterrey, CA, September 2002.

4. Atienza, D. V. *Characterization of Noise Technology Radar (NTR) Signal Detectability Using Non-Cooperative Receiver*. Master's thesis, Air Force Institute of Technology, GE-ENG-11-01, March 2011.

5. Gronholz, B. D. *Non-Cooperative Detection of Ultra Wideband Signals*. Master's thesis, Air Force Institute of Technology, GE-ENG-04-29, March 2004.

6. Mims, W. H. *Wideband Signal Detection Using a Down-Converting Channelized Receiver*. Master's thesis, Air Force Institute of Technology, GE-ENG-06-42, March 2006.

7. Szmajda, M, K. Gorecki and J. Mroczka, "Gabor Transform, Gabor-Wigner Transform and SPWVD as Time-Frequency Analysis of Power Quality. *Int'l Conf on Harmonics and Quality of Power* (ICHQP2010), Bergamo, Italy, Sep 2010.

8. Klein, R. W. ., M. A. Temple and M. J. Mendenhall, "Application of Wavelet-Based RF Fingerprinting to enhance wireless network security", *Jour of Communications and Networks*, Vol. 11, No. 6, Dec 2009.

9. IEEE 802.11-2005, *Local and Metropolitan Area Networks, Part 11: Wireless LAN Medium Access Control (MAC) and Physical Layer (PHY) specifications*. Inst of Electrical and Electronics Engineers, New York, New York, USA, Aug 2005.

10. Reising, D. R., M. A. Temple and M. E. Oxley, "Gabor-Based RF-DNA Fingerprinting for Classifying 802.16e WiMAX Mobile Subscribers". *Int'l Conf on Computing, Networking and Communications* (ICNC12), Maui, Hawaii, Jan 2012.

11. Reising, D. R. and M. A. Temple, "WiMAX Mobile Subscriber Verification Using Gabor-Based RF-DNA Fingerprints", *Int'l Communications Conference* (ICC12), Ottawa, Canada, Jun 2012.

12. *IEEE Std 802.16e-2005, Local and Metropolitan Area Networks, Part 16: Air Interface for Broadband Wireless Access System*. Inst of Electrical and Electronics Engineers, New York, New York, USA, Feb 2006. ISBN 0-7381-4857-1.

13. *BreezeMAX Extreme 5000: WiMAX 16e Pioneer for the License-Exempt Market*, Alvarion, Edition 215373 Rev. A, 2009.

REPORT DOCUMENTATION PAGE

Form Approved
OMB No. 0704-0188

1. REPORT DATE *(DD-MM-YYYY)*	2. REPORT TYPE	3. DATES COVERED *(From - To)*
22/03/2012	Master's Thesis	Aug 2010-Mar 2012

4. TITLE AND SUBTITLE

OFDM-BASED SIGNAL EXPLOTATION USING QUADRATURE MIRROR FILTER BANK (QMFB) PROCESSING

5a. CONTRACT NUMBER

5b. GRANT NUMBER

5c. PROGRAM ELEMENT NUMBER

6. AUTHOR(S)

Garrido, Felipe E., Captain, Chilean Air Force

5d. PROJECT NUMBER

5e. TASK NUMBER

5f. WORK UNIT NUMBER

7. PERFORMING ORGANIZATION NAME(S) AND ADDRESS(ES) AND ADDRESS(ES)

Air Force Institute of Technology
Graduate School of Engineering and Management (AFIT/ENG)
2950 Hobson Way
WPAFB OH 45433-7765

8. PERFORMING ORGANIZATION REPORT NUMBER

AFIT/GE/ENG/12-16

9. SPONSORING / MONITORING AGENCY NAME(S) AND ADDRESS(ES)

Letnic, Dalibor, Lt Col, Chilean Air Force
Chilean Air Force Mission
1100 17th Street N.W., Suite 900
Washington, D.C. 20036
(202)872-1335 x201

10. SPONSOR/MONITOR'S ACRONYM(S)

11. SPONSOR/MONITOR'S REPORT NUMBER(S)

12. DISTRIBUTION / AVAILABILITY STATEMENT

APPROVED FOR PUBLIC RELEASE; DISTRIBUTION UNLIMITED

13. SUPPLEMENTARY NOTES

14. ABSTRACT

By performing QMFB processing with a given signal it is possible to obtain Frequency-Time (F-T) outputs that represent signal features such as bandwidth (W), center frequency (f_c), signal duration (T_s), modulation type (AM, FM, BPSK, QAM, etc), frequency content and time allocation. Because of its unique structure, two widely used signals based on Orthogonal Frequency Division Multiplexing (OFDM) were chosen as signals of interest for demonstration. The general implementation of the QMFB process is described along with the basic structure of OFDM signals related to the physical layer perspective of 802.11a Wi-Fi and 802.16e WiMAX frame structures are described.

The adopted methodology is aimed at exploiting signal of interest features accounting for the effects of signal resampling and zero-padding. Computed simulation results are obtained after applying the defined methodology to each signal of interest. Initial time domain and frequency domain responses are presented for each input signal along with the initial and computed resampled parameters for each case. Results for selected QMFB outputs are presented using 2D F-T QMFB plots and 1D average frequency and average time plots. These plots enable qualitative visual assessment such as may be used by a human operator. The 1D responses are computed for the input signal and output QMFB responses and compared using overlay plots for single burst and multiple integrated burst inputs. Resultant time (Δt) and frequency (Δf) resolutions were consistent and validate the usefulness of QMFB processing.

15. SUBJECT TERMS

QMFB, OFDM, 802.11a Wi-Fi, 802.16e WiMAX

16. SECURITY CLASSIFICATION OF:			17. LIMITATION OF ABSTRACT	18. NUMBER OF PAGES	19a. NAME OF RESPONSIBLE PERSON
a. REPORT	b. ABSTRACT	c. THIS PAGE			Dr. Michael A. Temple
U	U	U	UU	104	19b. TELEPHONE NUMBER *(include area code)* 937-255-3636 x4279, michael.temple@afit.edu

Standard Form 298 (Rev. 8-98)
Prescribed by ANSI Std. Z39.18